CDF Note 5624, 2-May-2001

PRECISION ELECTROWEAK PHYSICS

Young-Kee Kim
University of California at Berkeley & LBNL
Berkeley, California 94720
E-mail: ykkim@lbl.gov

These three lectures given at TASI-2000 review the experimental state of electroweak interactions and the search for electroweak symmetry breaking.

1 Introduction

One of the central problems in particle physics is to understand the origin and values of the particle masses. In the Standard Model, particles acquire their masses by interacting with Higgs scalars. Thus uncovering the secrets of the Higgs sector is the focus of much present and future experimental research. The Higgs sector can be probed by the precision electroweak measurements such as M_Z, $\sin^2\theta_W$, M_W, and $M_{\rm top}$ by means of quantum corrections. However, the nature of the symmetry breaking sector can only be established by its direct discovery and detailed study.

The first lecture (Section 2) surveys the accelerators that produce heavy particles such as W, Z, and top quark, and the detectors that identify them and measure their properties. The second and third lectures review the precision measurements that probe the Higgs sector (Section 3) and the current and future searches of the Higgs boson (Section 4).

2 Survey of Accelerators and Detectors

2.1 Colliders versus Fixed-target machines

Suppose that we wish to study the Z boson. This requires a centre-of-mass energy of $\sim$90 GeV. In the e^+e^- symmetric collider (e^+ energy = e^- energy), this would require a beam energy of $\sim$45 GeV. Assuming a quark in a proton carries about 1/6 of the proton energy on average (see Figure 1), the proton and anti-proton collider would require a beam energy of $\sim$270 GeV.[a] In order to achieve the same goal, a proton fixed-target machine would require a proton beam energy of $\sim$20 TeV.

[a]Note that the energy loss due to synchrotron radiation is much larger for electrons than protons ($E_{sync} \sim 1/m^4$ in a circular accelerator ring), thus it is easier to accelerate protons than electrons.

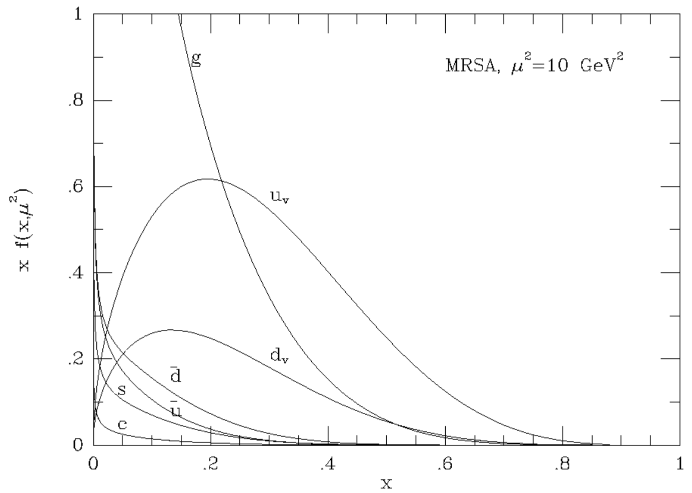

Figure 1: Quark and gluon energy distribution functions at $\mu^2 = 10$ GeV^2 where x is momentum fraction carried by a quark or gluon. Figure courtesy of "QCD and Collider Physics" by R.K. Ellis, W.J. Stirling and B.R. Webber.

With the great technological achievements of accelerator physics in colliding one high-energy beam with another, colliders satisfy our need to study elementary processes at high energies better than fixed target machines.

2.2 e^+e^- colliders versus Hadron colliders

The highest beam energy achieved in an e^+e^- collider is 104 GeV by LEP-2 (LEP stands for Large Electron Positron collider) at CERN, and the highest energy achieved in a hadron collider is 900 GeV [b] by the Tevatron at Fermilab. The beam energy in LHC (Large Hadron Collider), which will begin in about 2006, will be 7 TeV.

Since electrons are elementary particles, all of their energy can be available to produce new particles, thus energy upto 208 GeV is available at LEP-2. The available energy is much larger at the Tevatron hadron collider as demonstrated in Figure 2 although the cross-section rapidly decreases with the energy. With large luminosity, hadron colliders would be good machines to discover massive particles. Note that the 3 heaviest particles, W, Z, and top quark,

[b] For the upcoming Tevatron run (Tevatron Run II), the proton and anti-proton beam energy will be 980 GeV.

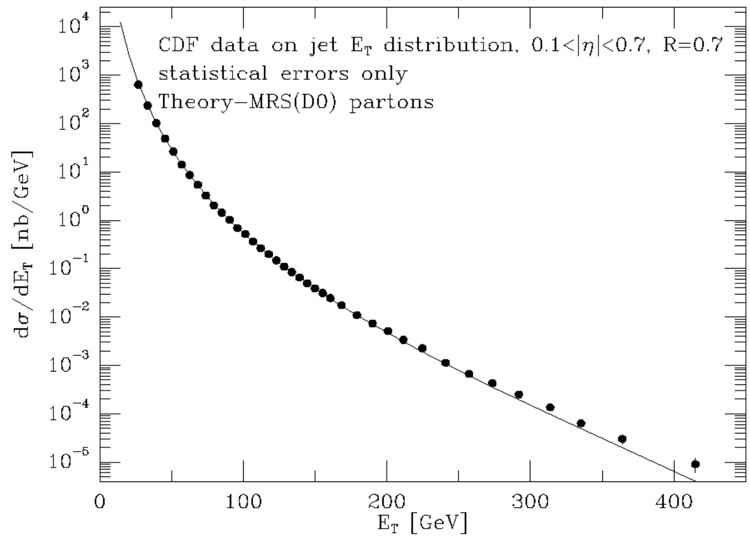

Figure 2: Jet E_T distribution from the CDF collaboration at the Tevatron.

were discovered at hadron colliders (see Table 1). [1,2] On the other hand, e^+e^- colliders have advantages such as their clean environment that makes precision measurements much easier and the fact that the final state particles are mostly detected so that the energy-momentum conservation can be used as a tool to improve the measurement resolution.

e^+e^- colliders and hadron colliders are thus complementary to each other.

2.3 Production of W, Z, and Top quark

Z production at LEP-1/SLC and W production at LEP-2

The experimental study of the process $e^+e^- \to Z \to f\bar{f}$:

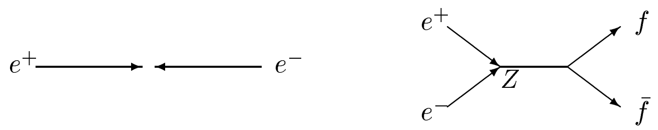

began in 1989 at LEP and SLC at SLAC. The LEP program completed data-taking at the Z resonance in 1995 (LEP-1), and the SLC program finished in

Table 1: Discovery of Fermions and Gauge Bosons

Type		Mass (GeV)	Discovery		
Lepton	e^-	0.00051	1898	J.J. Thomson	
	e^+	0.00051	1931	Anderson	cosmic ray
	μ	0.106	1937	Anderson et al	cosmic ray
	τ	1.777	1975	Martin Perl	e^+e^- collider
	ν_e	$\sim$0	1953	Cowan & Reines	fission reactor
	ν_μ	$\sim$0	1962	Lederman, Schwartz, Steinberger	p accelerator
	ν_τ	$\sim$0	2000	DONUT	p accelerator
Quark	d	0.003−0.009			
	u	0.001−0.005			
	s	0.075−0.170	1947	Rochester & Butler	cosmic ray
	c	1.15−1.35	1974	Mark I & BNL-E-0598	e^+e^- coll. & p accel.
	b	4.0−4.4	1977	FNAL-E-0288	p accelerator
	t	174.3±5.1	1995	CDF & DØ	$p\bar{p}$ collider
Gauge	γ	0			
Boson	g	0	1979	Tasso / Mark J	e^+e^- collider
	W	80.419±0.056	1982	UA1 & UA2	$p\bar{p}$ collider
	Z	91.188±0.002	1982	UA1 & UA2	$p\bar{p}$ collider

1998. The total LEP event sample consists of $15.5 \times 10^6 Z \to q\bar{q}$ and $1.7 \times 10^6 Z \to \ell^+\ell^-$ events collected at $\sim$7 energies about the Z mass. The total SLC sample consists of 557,000 events collected with left-handed and right-handed electron beams. Typical Z candidates recorded are shown in Figure 3.

Starting in 1996, LEP increased the beam energy to produce W boson pairs (LEP-2). Three diagrams contribute to the W pair production:

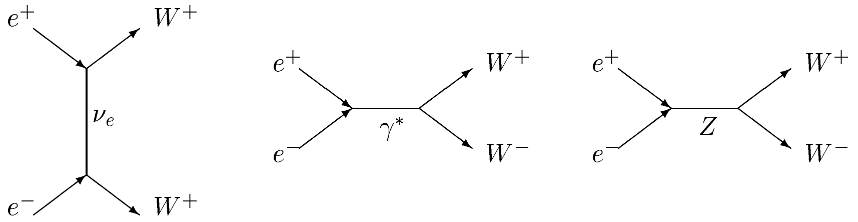

The neutrino exchange diagram dominates near the W pair threshold, $\sqrt{s} \simeq 2M_W \simeq 161$ GeV. As $\sqrt{s}$ increases, the contributions of the other two diagrams get larger, but there is a negative interference between them. This is illustrated in Figure 4, where the expected cross-section is shown with the full Standard Model structure, and if one or both of the diagrams with triple vector boson couplings is omitted, unitarity is violated. Figure 5 shows a W^+W^- candidate recorded at the LEP-2 experiments.

The cross sections in e^+e^- annihilation with $\sqrt{s}$ <700 GeV are summarized in Figure 6. Dominant processes are $e^+e^- \to \gamma^* \to f\bar{f}$ at $\sqrt{s} < M_Z$, $e^+e^- \to Z \to f\bar{f}$ at $\sqrt{s} \simeq M_Z$, and $e^+e^- \to W^+W^-$ at $\sqrt{s} > 200$ GeV.

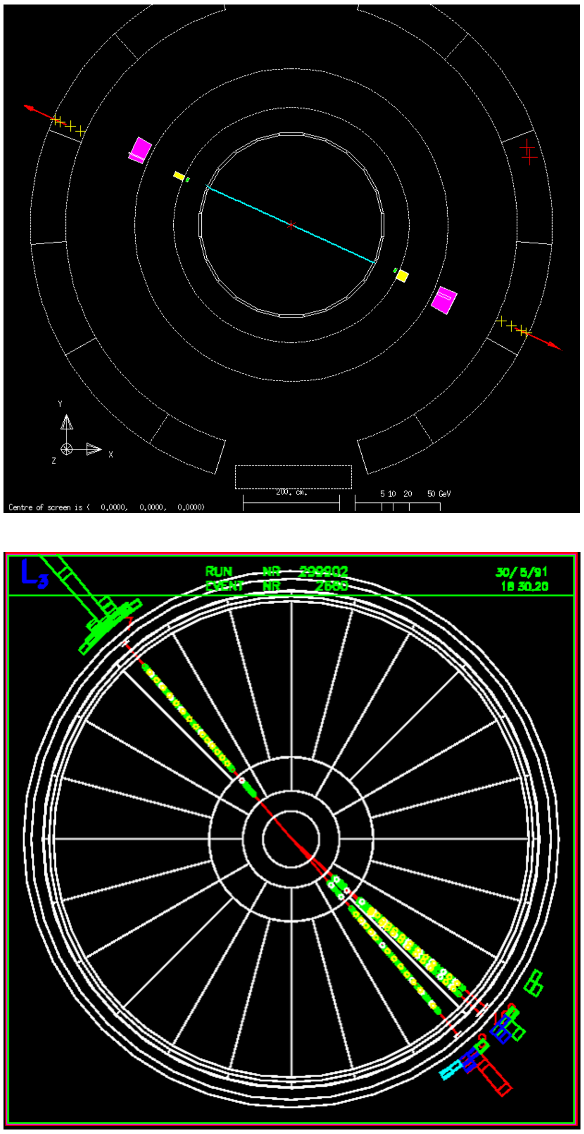

Figure 3: An $e^+e^- \to Z \to \mu^+\mu^-$ candidate (Top) recorded at the OPAL experiment and an $e^+e^- \to Z \to \tau^+\tau^-$ candidate (Bottom) recorded at the L3 experiment at LEP-1.

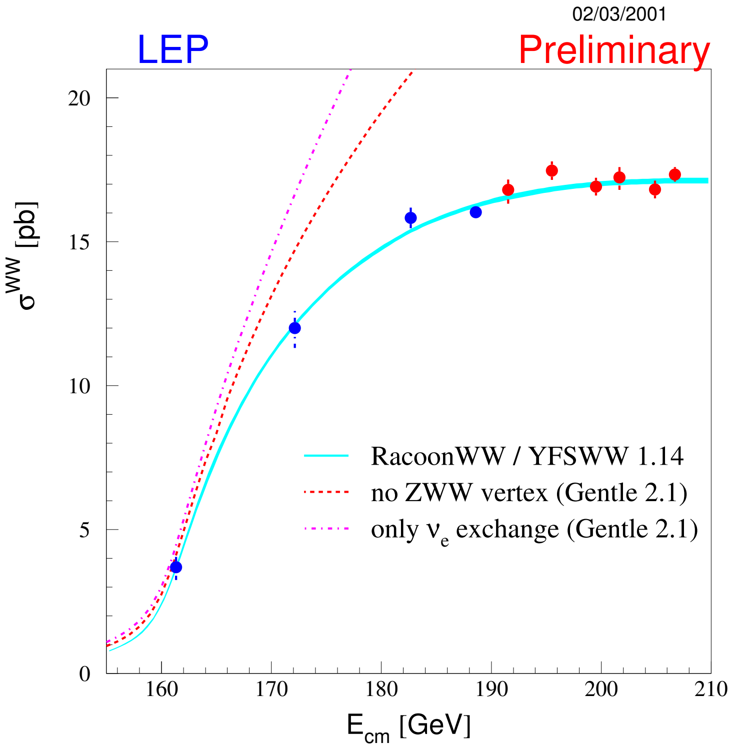

Figure 4: LEP-2 average W pair production cross-section, corrected to correspond to the three doubly-resonant W production diagrams.

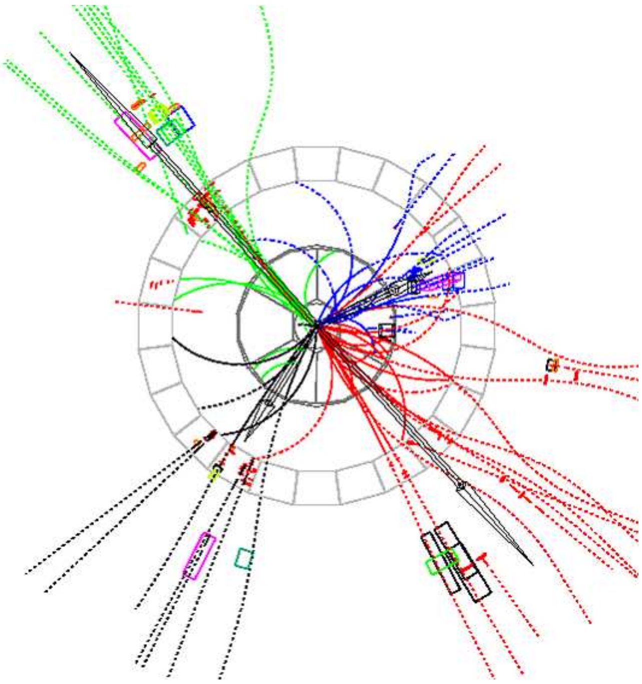

Figure 5: An $e^+e^- \to W^+W^-$ candidate recorded at the DELPHI experiment at LEP-2, where W^+ and W^- decays each into a pair of quarks giving a four jet topology.

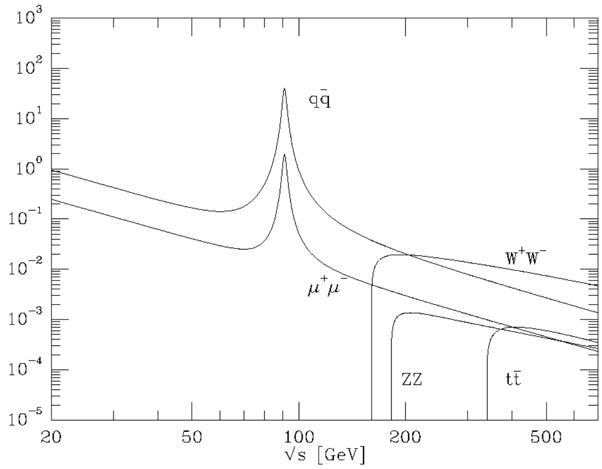

Figure 6: Cross sections in e^+e^- annihilation.

Z and W production at the Tevatron

The primary production of Z and W bosons at the Tevatron arises from the reactions: $u\bar{u} \to Z$, $d\bar{d} \to Z$, $u\bar{d} \to W^+$, and $\bar{u}d \to W^-$, where the up and down quarks (and antiquarks) can be valence or sea quarks in the proton [c]:

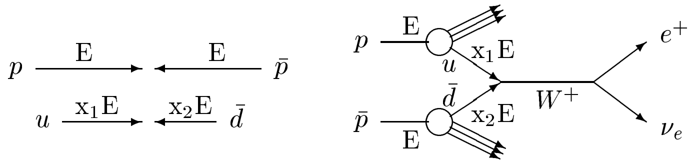

Although both Z and $W^{\pm}$ are produced through quark-antiquark annihilation, the dominant contribution is not from the valence-valence collisions but from valence-sea collisions. The typical $q\bar{q}$ center-of-mass energy $\sqrt{\hat{s}}$ for W, Z production is the mass of the boson, $\sqrt{\hat{s}} \sim M_{Z,W}$. Since these boson masses are around 100 GeV, about 1/20 of the $p\bar{p}$ center-of-mass energy, both valence and sea quarks have a good probability for carrying a sufficient fraction of the proton's energy to produce a gauge boson (see Figure 1). The valence-sea production mechanism is about 4 times larger than the valence-valence and sea-sea production mechanisms. It is coincidental that the valence-valence and sea-sea mechanisms are about equal at this energy. At higher energies such as LHC, the sea-sea mechanism dominates; at lower energies such as $Sp\bar{p}S$ where the center-of-mass energy was 560 GeV, the valence-valence mechanism dominates.

Top-quark production at the Tevatron

The Tevatron has been (and will be until LHC turns on) the unique place to produce top quarks. The dominant top-quark production mechanism at the Tevatron is the annihilation of the valence quark and the valence antiquark into a gluon, which then decays into a $t\bar{t}$ pair. One of the $t\bar{t}$ cadidates recorded at the Tevatron is shown in Figure 7. The dominant top-quark production mechanism at the LHC (proton-proton collider) will be the annihilation of a gluon and a gluon into a gluon, which in turn decays into a $t\bar{t}$ pair.

[c] The proton consists of three *valence* quarks *(uud)* which carry its electric charge and baryon quantum numbers, and an infinite *sea* of light $q\bar{q}$ pairs.

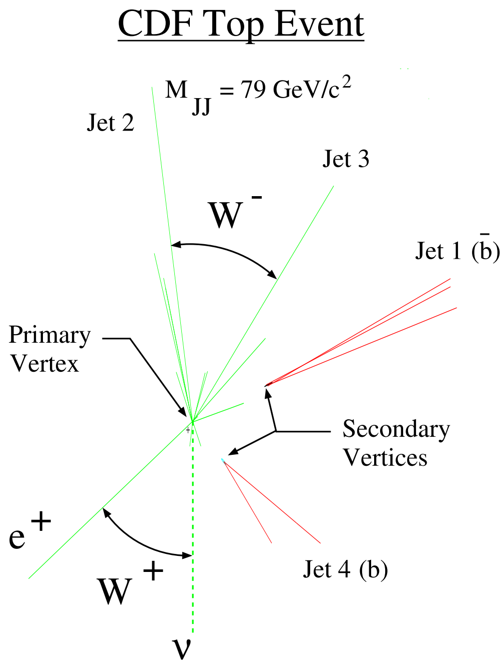

Figure 7: A $t\bar{t}$ candidate recorded at the CDF experiment, where $t \to W^+b \to e^+\nu b$ and $\bar{t} \to W^-\bar{b} \to q\bar{q}\bar{b}$.

Summary

Table 2 summarizes the number of W, Z and $t\bar{t}$ events identified at LEP-1, LEP-2, SLC and the Tevatron.

2.4 Survey of W, Z, and Top quark Properties

The W, Z, and top particles (and the other elementary particles in the Standard Model) are structureless upto our current resolution, which is about 10^{-16} – 10^{-17} cm; Note that the top-quark mass is enormous, as heavy as a gold atom which consists of 79 protons and 118 neutrons and yet it is structureless. Coincidentally the top-quark mass is about the sum of the Z boson mass and the W boson mass. The top quark and W and Z bosons decay immediately after they are produced; their lifetimes, provided by their width measurements, are

Table 2: The number of W's, Z's and top quarks.

Heavy Particle	Accelerator	C.M. Energy	# of events
Z	LEP-1	~91 GeV	17,221,000
	SLC	~91 GeV	557,000
	Tevatron	1.8 TeV	9,000
W	LEP-2	132 ~ 208 GeV	10,000
	Tevatron	1.8 TeV	180,000
top	Tevatron	1.8 TeV	100

around 10^{-25} sec. With current date techniques, we can not trace their decays in space.

Z's decay into a fermion (a quark or a lepton) and its anti-fermion, and W's decay into a fermion and its weak interaction partner: $W^+ \rightarrow e^+\nu_e$, $\mu^+\nu_\mu$, $\tau^+\nu_\tau$, $u\bar{d}$, and $c\bar{s}$. Top quarks decay about 100% of time into a W and a b quark, the weak interaction partner of the top quark ($t \rightarrow W^+b$). B hadrons (hadrons containing b quarks) live long, 1.5×10^{-12} s, at the elementary particle scale. For instance, b quarks from the top decay which have a momentum of ~50 GeV travel about 4 mm before decaying, which is large enough to trace down in space. This is demonstrated in Figure 7 by the displaced vertices (seconary vertices).

2.5 Detectors

In order to identify various types of particles such as electrons, muons, taus, neutrinos, and b-quarks, which are the products of Z, W, and top decays, a typical experimental detector consists of layers of devices as shown in Figure 8. Imagine you are riding on a particle that was just produced by the collision of a proton and an anti-proton or an electron and a positron. It encounters a thin beam pipe. It then zips through a silicon device, capable of resolving very tiny distances (~100 μm), thus identifing b-quarks in the event as shown in Figure 7. After the silicon device, it zips through a gas containing an immense number of very thin gold wires. The particle passes ~100 of these wires. If the particle is charged, each nearby wire records its passage, and the particle's path is determined (see Figures 3,5,7). A measurement of the curvature (this device and the silicon device are typically inside of magnetic field B produced by a solenoid) gives us the momentum of the particle:

$$p = \frac{qBr}{c},$$

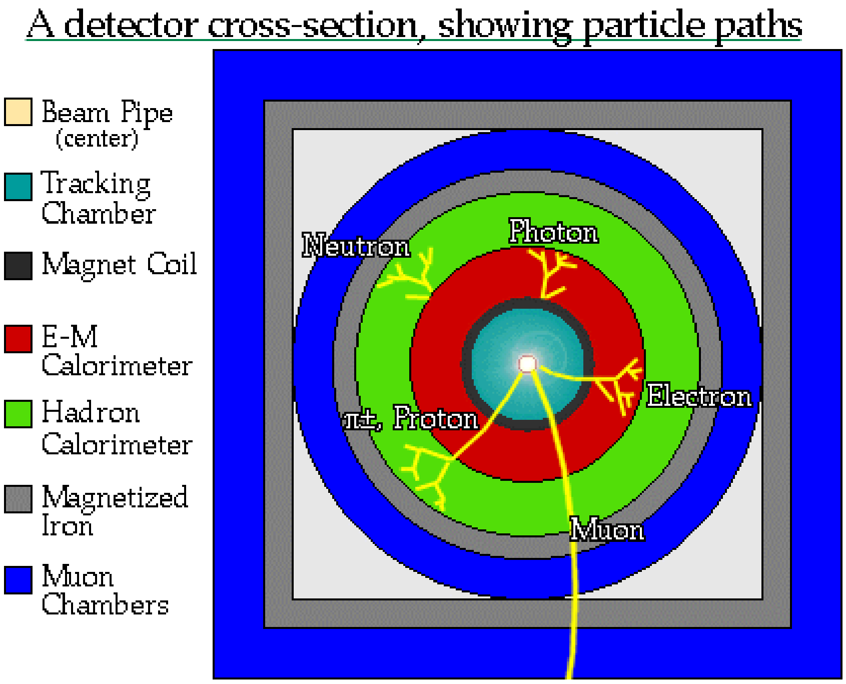

Figure 8: The beam's view of a typical detector.

where q is the charge of the particle, r is the inverse curvature, and c is the speed of light. If the particle is neutral, there will be no signal on the wire. Next the particle passes through coil of solenoid magnets. It then passes into a calorimeter section, which measures particle energy except muons and neutrinos. Different particles interact differently with matter, thus with calorimeter. If an electron, it fragments on a series of closely spaced thin lead plates and scintillator between the plates, giving up its entire energy in 3 or 4 inches. If a hadron, it penetrates 10 to 20 inches of calorimeter material before exhausting all of its energy through nuclear collisions. If it is a muon, it zips through the calorimeter sections and leaves hits in a gas containing thin gold wires which is located outside of the calorimeter. Neutrinos leave the detector entirely, leaving behind not even a hint of their fragrance. The system stores the data with about one million bits of information for each event.

3 Precision Electroweak Measurements

3.1 Tree-level formulation

QED can be described by one parameter e or $\alpha = e^2/(4\pi)$ where $1/\alpha = 137.03599959(38)(13)$, most precisely derived from $g-2$ measurements. [3] In the electroweak theory, the strengths are specified by three paramters. They are two gauge coupling constants g and g', and v, the vacuum expectation value of the Higgs field (see Chris Quigg's lectures in this proceedings). These three parameters as inputs predict charges, M_W, M_Z, and G_F via the following relationships:

$$\sin^2\theta_W = 1 - \frac{M_W^2}{M_Z^2} \tag{1}$$

$$= \frac{\pi\alpha}{\sqrt{2}G_F M_W^2} \tag{2}$$

$$= \frac{e^2}{g^2} \tag{3}$$

$$= 1 - \frac{e^2}{g'^2}. \tag{4}$$

The theory is democratic so that any three variables in the above equations may be chosen as inputs. It makes much more sense to choose the three parameters most accurately measured so that the predictions for any other measurements become as precise as possible, allowing sensitive tests of the theory. In the early 1980s, those were e (or α), G_F [d] and the electroweak-mixing parameter $\sin^2\theta_W$. With the measured values of these parameters, the masses of the W and Z bosons were prediced to be around 80 GeV and 90 GeV, respectively. This prediction lead to the discovery of the W and Z boson at $Sp\bar{p}S$ at CERN.[1] By the end of August 1989, the 4 LEP experiments measured M_Z to within 160 MeV. Since then, α, G_F and M_Z were adopted as the basic input parameters. The current M_Z accuracy by LEP is 2 MeV (0.002%). [4] Most likely, this measurement won't be improved in the near future.

3.2 Higher Order Corrections

Once higher order corrections are included, all these equalities are no longer exactly true. In gauge theories, higher order corrections such as the loop diagrams lead to infinities which require renormalization. A general consequence

[d] $G_F = (1.16637 \pm 0.00001) \times 10^{-5}$ GeV^{-2} is derived from the muon lifetime measurements using the radiative corrections of the $V-A$ Fermi theory.

of this is the introduction of Q^2 dependent corrections to the parameters of the theory, therefore corrections to the relationships among the parameters.

For instance, the Born level relationship

$$\mathrm{G_F} = \frac{\pi\alpha}{\sqrt{2}\mathrm{M_W^2}}\frac{\mathrm{M_Z^2}}{\mathrm{M_Z^2}-\mathrm{M_W^2}} \tag{5}$$

will be modified by

$$\mathrm{G_F} = \frac{1}{1-\Delta\mathrm{r}}\frac{\pi\alpha}{\sqrt{2}\mathrm{M_W^2}}\frac{\mathrm{M_Z^2}}{\mathrm{M_Z^2}-\mathrm{M_W^2}} \tag{6}$$

in higher orders. Here

$$\Delta r \sim \Delta r_0 - \rho_t/\tan\theta_W \tag{7}$$

$$\Delta r_0 \simeq 1-\alpha(0)/\alpha(M_Z) \simeq 0.06 \tag{8}$$

$$\rho_t = \frac{3\mathrm{G_F M_t^2}}{8\sqrt{2}\pi^2} \simeq 0.0096[\frac{\mathrm{M_t}}{175\mathrm{GeV}}]^2 \tag{9}$$

where $\alpha(M_Z)$ is the electromagnetic coupling constant at the scale of the Z mass and the top quark contributes ρ_t. As shown in Δr_0, the bulk of the corrections can be observed in "running" (Q^2-dependent) coupling. The uncertainty in $\alpha(M_Z)$ is dominated by the contribution of the light quarks (u through b), $\Delta\alpha_{had}^{(5)}(M_Z^2)$ [12] :

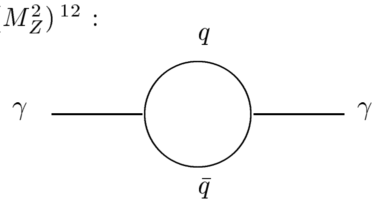

This is evaluated using dispersion relations and $\sigma(e^+e^- \to \text{hadrons})$ measurements at low $\sqrt{s}$, and perturbative QCD calculations at large $\sqrt{s}$.

The relationship can also be written as

$$[\frac{M_W}{M_Z cos\theta_W}]^2 = 1 \tag{10}$$

in the lowest order, and

$$\begin{aligned}[\frac{M_W}{M_Z cos\theta_W}]^2 &\simeq 1 + \frac{3G_F M_t^2}{8\sqrt{2}\pi^2} \\ &\simeq 1 + 0.0096\,[\frac{M_t}{175GeV}]^2\end{aligned} \tag{11}$$

with higher order corrections. The second term in this equation (or ρ_t in Eq. 9) is contributed by the top quark in loop diagrams:

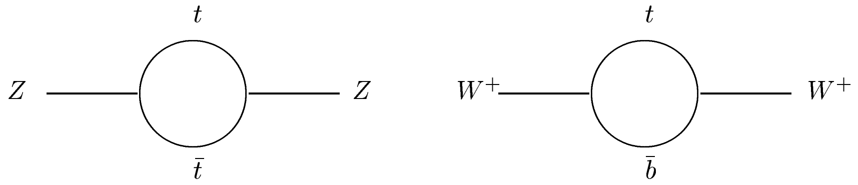

With $M_{top} \sim 175$ GeV, the correction is about 1% level. Thus precision measurements of M_W, M_Z, and $\cos\theta_W$ with much better than 1% accuracy can predict the top-quark mass. The predicted top mass from electroweak measurements is $M_{top} = 172^{+14}_{-11}$ GeV.[4] The top mass measured by the CDF and DØ Tevatron experiments is $M_{top} = 174.3 \pm 5.1$ GeV,[5] which agrees with the prediction very well. This is a good example of the successful interplay between theory and experiments. Any inconsistency between the predicted and measured values would have hinted at new physics.

Secondary contributions to electroweak observables (or to Eq. 11) are from the Higgs boson in loop diagrams

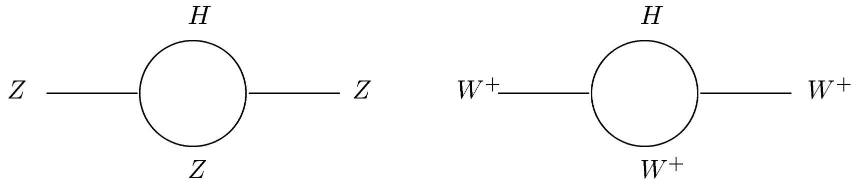

which are proportional to

$$\ln(\mathrm{M_H^2/M_W^2})$$

where the Higgs mass M_H is unknown in the Standard Model. New particles beyond the Standard Model could also contribute to electroweak observables through loop diagrams. Difficulties arise due to these unknown masses, M_H and $M_{\text{new particle}}$. This could be bad news since the predictions are uncertain and it is hard to test the theory. Or this could be good news since the predictions depend on the unknown masses. Indeed precision measurements provide information about these unknown masses of particles which are too heavy to be produced directly, or whose production cross section is too small to be observed. For example, with ~30 MeV uncertainty in M_W and ~2 GeV uncertainty in M_{top}, we can predict the Higgs boson mass within ~30%. When precision measurements are inconsistent each other (for example, different sets of precision measurements predict different Higgs masses), this may signal the presence of new physics beyond the Standard Model.

3.3 The Experimental Inputs

The last decade has been a remarkable improvement in our knowledge of various electroweak parameters. Much of the improvement is due to the study of the Z resonance at LEP-1 and the SLC, and the study of W and top quark at LEP-2 and the Tevatron.

Z boson parameters

The precise determination of the Z boson parameters from the measurements at the Z resonance by the four collaborations ALEPH, DELPHI, L3 and OPAL in e^+e^- collisions at LEP and by the SLD collaboration in e^+e^- collisions at the SLC is a landmark for precision tests of the electroweak theory.

Cross section at the Z peak

The coupling of the Z to a fermion (f) and an anti-fermion ($\bar{f}$) pair is described by the following Lagrangian density,

$$L = (\frac{G_F M_Z^2}{2\sqrt{2}})^{1/2} \bar{\Psi}_f \gamma_\mu (v_f - a_f \gamma_5) \Psi_f Z^\mu \tag{12}$$

$$= (\frac{G_F M_Z^2}{2\sqrt{2}})^{1/2} \bar{\Psi}_f \gamma_\mu [g_L^f (1-\gamma_5) + g_R^f (1+\gamma_5)] \Psi_f Z^\mu \tag{13}$$

where v_f and a_f are vector and axial vector coupling constants, and $g_L^f = (v_f + a_f)/2$ and $g_R^f = (v_f - a_f)/2$ are left-handed and right-handed combinations. The vector and axial vector couplings are related to the quantum numbers of the fermion as follows

$$v_f = \sqrt{\rho_f}(2I_3^f - 4Q_f \sin^2\theta_f) \tag{14}$$

$$a_f = \sqrt{\rho_f}(2I_3^f) \tag{15}$$

where I_3^f is the third component of weak isospin, Q_f is the electric charge, and the parameters $\rho_f \sim 1$ and $\sin^2\theta_f \sim 0.23$ incorporate electroweak radiative corrections.

The cross section for the process $e^+e^-(P_e) \to Z \to f\bar{f}$ is described in the center-of-mass frame by the following expression,

$$\frac{d\sigma_Z^{f\bar{f}}}{d\Omega} = \frac{9}{4} \frac{s\Gamma_{ee}\Gamma_{f\bar{f}}/M_Z^2}{(s-M_Z^2)^2 + s^2\Gamma_Z^2/M_Z^2} \tag{16}$$
$$[(1+\cos^2\theta)(1-P_e A_e) + 2\cos\theta A_f(-P_e + A_e)]$$

where P_e is the polarization of the electron beam, s is the square of the center-of-mass energy, Γ_Z is the total width of the Z, θ is the angle between the incident electron and the outgoing fermion, $\Gamma_{f\bar{f}}$ is the partial width for $Z \to f\bar{f}$, and A_f is the left-right coupling constant asymmetry. The partial widths and coupling constant asymmetries are related to the couplings defined in the Lagrangian,

$$\Gamma_{f\bar{f}} = N_c \cdot \frac{G_F M_Z^3}{24\pi\sqrt{2}}(v_f^2 + a_f^2)(1+\delta) \tag{17}$$

$$A_f = \frac{2v_f a_f}{v_f^2 + a_f^2} = \frac{(g_L^f)^2 - (g_R^f)^2}{(g_L^f)^2 + (g_R^f)^2}, \tag{18}$$

where $\delta \simeq 1 + 3\alpha Q_f^2/4\pi + n_f \alpha_s/\pi$, ($n_f$ is 1 for quarks and 0 for leptons) accounts for final state QED and QCD radiative effects.

The small size of $v_\ell/a_\ell(\sim 0.08)$, where $\ell = e, \mu, \tau$, makes the leptonic coupling asymmetries A_ℓ particularly sensitive to electroweak vacuum polarization corrections. The leptonic asymmetries are usually parameterized in terms of $\sin^2\theta_W^{eff} = \sin^2\theta_\ell$ (assuming lepton unversality). It follows that small changes in $\sin^2\theta_W^{eff}$ produce large effects on A_ℓ,

$$A_\ell = \frac{2(1 - 4\sin^2\theta_W^{eff})}{1 + (1 - 4\sin^2\theta_W^{eff})^2} \tag{19}$$

$$\delta(A_\ell) \simeq -8 \cdot \delta(\sin^2\theta_W^{eff}). \tag{20}$$

Electroweak Observables at the Z pole

The cross section described in Eq. 16 is only the dominant term in the total s-channel e^+e^- cross section which can be expressed as

$$\frac{d\sigma_{tot}^{f\bar{f}}(s)}{d\Omega} = \frac{d\sigma_\gamma^{f\bar{f}}(s)}{d\Omega} + \frac{d\sigma_{\gamma Z}^{f\bar{f}}(s)}{d\Omega} + \frac{d\sigma_Z^{f\bar{f}}(s)}{d\Omega}, \tag{21}$$

where the first and second terms represent photon exchange, and the interference between photon and Z diagrams, respectively. At $\sqrt{s} = 30 - 40$ GeV (the centre-of-mass range for the PEP and PETRA colliders), the dominant contribution comes from $\sigma_\gamma^{f\bar{f}}$ and the $\sigma_{\gamma Z}^{f\bar{f}}$ contribution to the total cross section is about $2 - 3\%$. At $\sqrt{s} \sim 60$ GeV (the centre-of-mass range for the TRISTAN collider), the $\sigma_{\gamma Z}^{f\bar{f}}$ contribution to the total cross section increases to about 25%. The contribution from $\sigma_Z^{f\bar{f}}$ is negligible in both cases. The cross section

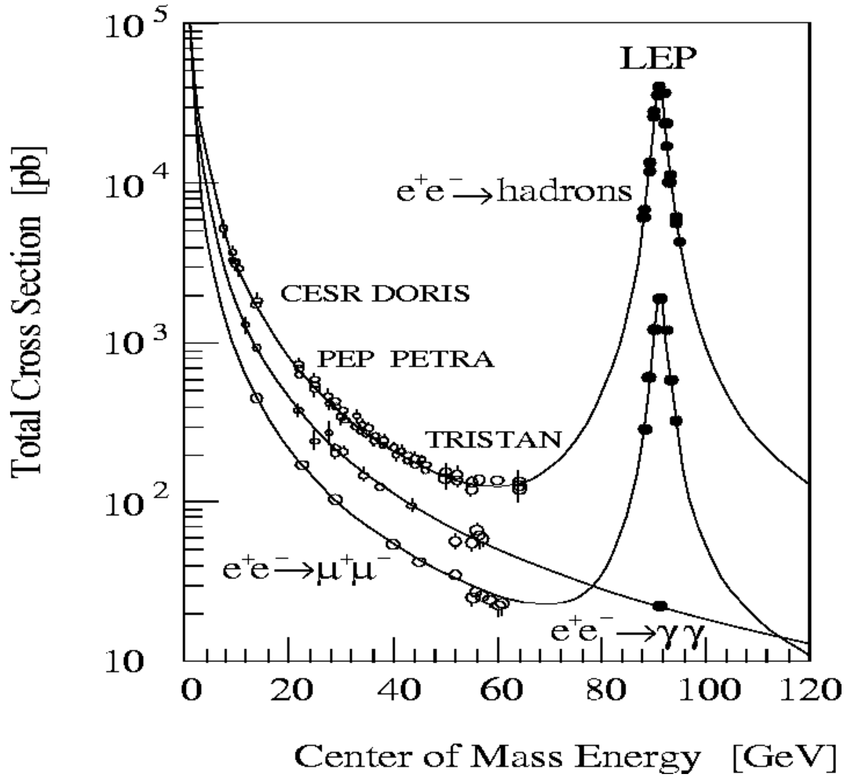

Figure 9: Cross-section of $e^+e^- \to f\bar{f}$.

near $\sqrt{s} = M_Z$ does not differ dramatically from the resonance cross section given in $\sigma_Z^{f\bar{f}}$ because the $Z - \gamma$ interference term vanishes at the pole, and the photon exchange cross section is approximately 1000 times smaller than the Z-exchange cross section. The cross-section measurements for fermion pair production from e^+e^- annihilation at $\sqrt{s} < 120$ GeV are summarized in Figure 9; the agreement between the measurements and the Standard Model predictions are excellent.

Using the information contained in hadronic and leptonic cross sections around the Z pole, it is possible to define a number of experimental observables:

1. The line shape parameters, which consists of the M_Z and Γ_Z whre the definition is based on the Breit-Wigner denominator $(s - M_Z^2 + is\Gamma_Z/M_Z)$ with s-dependent width, and the peak hadronic cross section σ_h^o (see

Figure 10)

$$\sigma_h^o = 12\pi\Gamma_{ee}\Gamma_{had}/(M_Z^2\Gamma_Z^2); \tag{22}$$

2. The cross section ratios

$$R_\ell = \Gamma_\ell/\Gamma_{had},\ R_b = \Gamma_{bb}/\Gamma_{had},\ R_c = \Gamma_{cc}/\Gamma_{had} \tag{23}$$

   where $\ell = e,\ \mu,\ \tau$;

3. The unpolarized forward-backward asymmetries

$$A_{FB}^f = \frac{\sigma_F^f - \sigma_B^f}{\sigma_F^f + \sigma_B^f} = 0.75 A_e A_f, \quad f = \ell, b, c \tag{24}$$

   where σ_F^f is the cross section for finding the scattered fermion in the hemisphere defined by the incident electron direction and σ_B^f is the cross section for finding it in the positron hemisphere;

4. The left-right asymmetry which is defined as

$$P_e A_{LR} = P_e A_e = \frac{\sigma^f(-|P_e|) - \sigma^f(+|P_e|)}{\sigma^f(-|P_e|) + \sigma^f(+|P_e|)}, \quad f \neq e \tag{25}$$

   where $\sigma^f(P_e)$ is the total cross section for the production of $f\bar{f}$ pairs with an electron beam of helicity P_e;

5. The polarization of final state τ-leptons which depends upon the direction of the τ, A_e, and A_τ,

$$P_\tau(\cos\theta) = -\frac{A_\tau(1+\cos^2\theta) + 2A_e\cos\theta}{1+\cos^2\theta + 2A_\tau A_e\cos\theta}; \tag{26}$$

6. The left-right forward-backward asymmetries

$$\begin{aligned} \tilde{A}_{FB}^f &= \frac{\sigma_F^f(-|P_e|) - \sigma_B^f(-|P_e|) - \sigma_F^f(+|P_e|) + \sigma_B^f(+|P_e|)}{\sigma_F^f(-|P_e|) + \sigma_B^f(-|P_e|) + \sigma_F^f(+|P_e|) + \sigma_B^f(+|P_e|)} \\ &= 0.75 P A_f, \quad f = \ell, s, c, b. \end{aligned} \tag{27}$$

The presence of initial-state QED radiation smears the center-of-mass energy. With the initial state QED corrections, $\sqrt{s}$ is reduced and σ changes. On the Z resonance, the cross-section is reduced by $\sim$30%, as demonstrated in Figure 10.

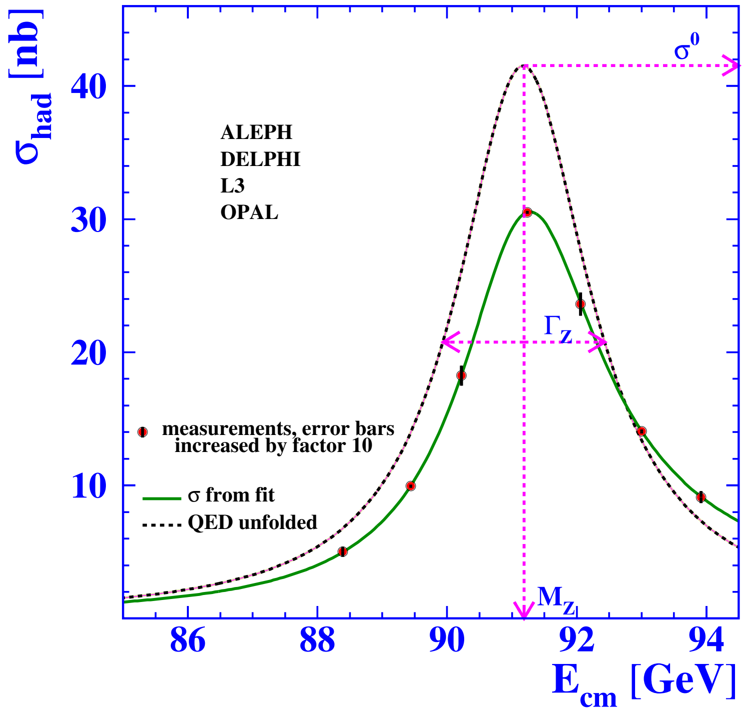

Figure 10: Average over measurements of the hadronic cross-sections by the four experiments, as a function of centre-of-mass energy. The dashed curve shows the QED deconvoluted cross-section, which defines the Z parameters.

The net correction to τ-polarization and the left-right asymmetry is less than 2%, and that to the leptonic forward-backward asymmetries is about 100%.

A summary of the combined LEP-1 results is presented in Table 3.[4] Note the remarkable precision of these measurements, especially the Z mass which is measured to 2.2×10^{-5}. It is the third most precisely determined electroweak parameter and used as an input to the theory.

The measurement of the left-right cross section asymmetry (A_{LR}) by SLD at the SLC provides a systematically precise, statistics-dominated determination of the coupling A_e, and is presently the most precise single measurement, with the smallest systematic error, of this quantity. In principle the analysis is straightforward: one counts the numbers of Z bosons produced by left and right longitudinally polarized electrons ($N_Z(L)$ and $N_Z(R)$), forms an asymmetry, and then divides by the e^- beam polarization magnitude (the e^+ is not

Table 3: Summary of the Z parameter measurements at LEP-1 and SLC. The middle box shows the combined result of the LEP lineshape analyses. R_ℓ and $A_{FB}^{0,\ell}$ assumed lepton universality. The bottom box presents the result from the SLC analysis.

Z parameter	Average Value
LEP-1	
M_Z	91.1875 ± 0.0021 GeV
Γ_Z	2.4952 ± 0.0023 GeV
σ_h^0	41.540 ± 0.037 nb
R_ℓ	20.767 ± 0.025
$A_{FB}^{0,\ell}$	0.0171 ± 0.0010
A_τ	0.1439 ± 0.0042
A_e	0.1498 ± 0.0048
$\sin^2\theta_{eff}^{lept}$	0.2321 ± 0.0010
SLC	
$\sin^2\theta_{eff}^{lept}$	0.23098 ± 0.00026

polarised):

$$A_{LR} = \frac{1}{P_e}\frac{N_Z(L) - N_Z(R)}{N_Z(L) + N_Z(R)}. \tag{28}$$

The average electron polarization at the interaction point has been in the range 73% to 77%. The measured value of A_{LR} [4] can be translated into the value of

$$\sin^2\theta_{eff}^{lept} = 0.23098 \pm 0.00026. \tag{29}$$

The decays of the Z to neutrinos are invisible in the detectors and give rise to the "invisible width", $\Gamma_{inv} = N_\nu \Gamma_{\nu\nu}$, where N_ν is the number of light neutrino species. The invisible width can be determined from the measurements of the decay widths to all visible final states and the total width, which is given by the sum over all partial widths,

$$\Gamma_Z = \Gamma_{ee} + \Gamma_{\mu\mu} + \Gamma_{\tau\tau} + \Gamma_{had} + \Gamma_{inv}. \tag{30}$$

The ratio of the invisible and leptonic widths is found to be

$$\Gamma_{inv}/\Gamma_{\ell\ell} = 5.941 \pm 0.016. \tag{31}$$

Dividing this number by the Standard Model value for the ratio of neutrino and leptonic widths $\Gamma_{\nu\nu}/\Gamma_{\ell\ell} = 1.9912 \pm 0.0012$ yields the number of light neutrinos,

$$N_\nu = 2.9835 \pm 0.0083 \tag{32}$$

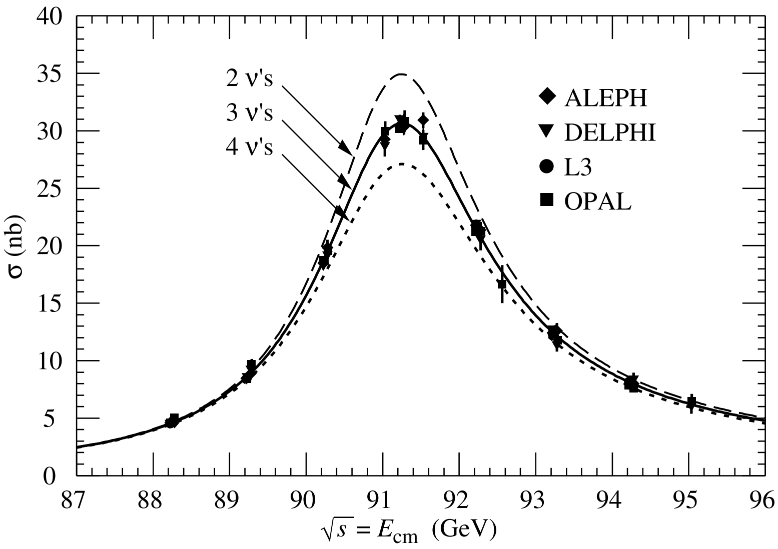

Figure 11: The Z lineshape at LEP-1. The three curves represent the predicted lineshapes with the assumption of two (dashed line), three (solid line), and four (dotted line) light neutrinos.

(see Figure 11). Note that N_ν is about 2σ less than the expected value of 3. Assuming that the number of light neutrinos is 3, the invisible width is converted into a 95% upper limit on an additional invisible width $\Delta\Gamma_{inv}$,

$$\Delta\Gamma_{inv} < 2.0 \text{ MeV}. \tag{33}$$

The accuracy of the measurements makes them sensitive to the mass of the top quark and to the mass of the Higgs boson through loop corrections as stated in section 3.2. An example of such sensitivity is presented in Figure 12. Predicted values from all the Z parameters are

$$M_W = 80.374 \pm 0.034 \text{ GeV}, \tag{34}$$

$$M_{top} = 169^{+10}_{-8} \text{ GeV}, \tag{35}$$

$$M_H = 56^{+75}_{-27} \text{ GeV}. \tag{36}$$

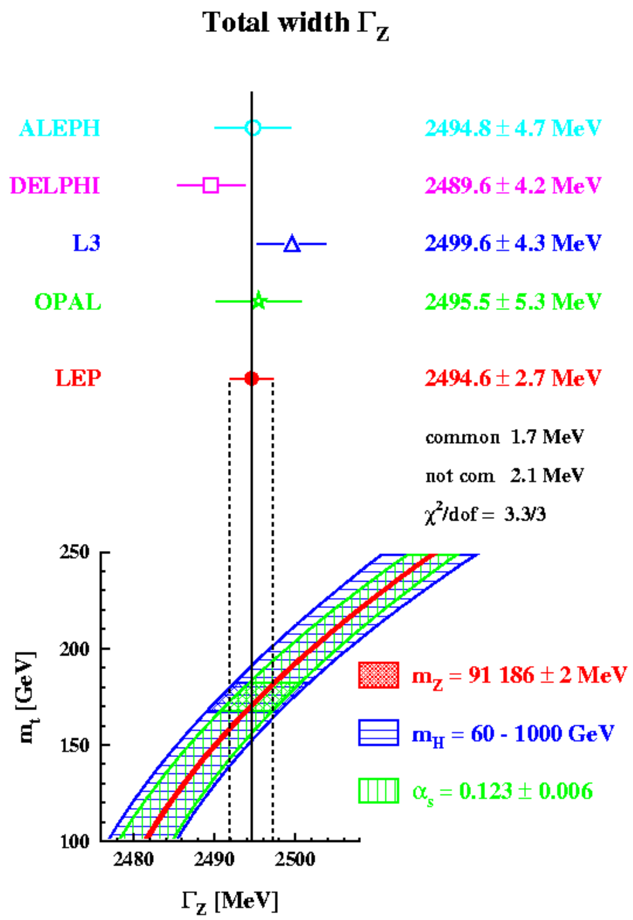

Figure 12: Summay of the Z width measurements at LEP-1 and the sensitivity of the Z width to the mass of the top quark.

Table 4: Typical W pair event selection efficiencies and purities.

Decay mode	Efficiency	Purity
$WW \to q\bar{q}q\bar{q}$	90%	80%
$WW \to q\bar{q}\ell\nu$	82%	90%
$WW \to \ell\nu\ell\nu$	$60 - 80\%$	90%

W boson parameters

The precise determination of the W boson and top-quark parameters was initiated by the CDF and DØ collaborations at the Tevatron. Since 1996, the LEP-2 program made a significant contribtuion on the W parameters. These make complementary tests of the Standard Model to those of LEP-1 and SLC. Together with the Z parameters, efforts to constrain M_H have become increasingly interesting.

W branching fractions, W mass and width from LEP-2 at CERN

By doubling the e^+e^- collision energy, LEP-2 provided a sample of W pair events. The typical selection efficiencies and purities for W pair events at LEP-2 are given in Table 4. The branching fractions for W decays via the electron, muon, tau, and hadronic modes have been measured by all four experiments [4]. The LEP-2 average results are given in Table 5. The results for the individual leptonic channels are consistent with lepton universality, and the average leptonic branching fraction $(10.74 \pm 0.10)\%$ is also consistent with the Standard Model expectation.

The leptonic W branching fraction can be re-interpreted in terms of the CKM matrix element V_{cs} without need for a CKM unitarity constraint, using the relatively well-known values of other CKM matrix elements involving light quarks [6]. These indirect constraints currently lead to a value [4] of $|V_{cs}| = 0.989 \pm 0.016$, much more precise than the value derived from D decays of 1.04 ± 0.16 [6].

The W mass can be extracted from the measurement of the W pair cross section at the W pair threshold, $\sqrt{s} \simeq 2M_W$. See the measurement point at $\sqrt{s} = 161$ GeV in Figure 4. The value of $\sqrt{s} = 161$ GeV was chosen from the 1995 Tevatron M_W measurement. At center-of-mass energies above the W pair threshold, the technique for measuring the W mass lies in the reconstruction of the directions and energies of the four primary W decay products. These may be either four quarks, approximated by four jet directions and energies, for the $q\bar{q}q\bar{q}$ channel; or two quarks (or two jets) and a charged lepton for the

Table 5: LEP average W decay braching fraction measurements.

Decay mode	Branching fraction (%)
$WW \to e\nu$	10.62 ± 0.20
$WW \to \mu\nu$	10.60 ± 0.18
$WW \to \tau\nu$	11.07 ± 0.25
$WW \to q\bar{q}$	67.78 ± 0.32

$q\bar{q}\ell\nu$ channel, deducing the neutrino direction and energy from the missing momentum in the event:

$$\vec{P}(e^+) + \vec{P}(e^-) = 0 = \vec{P}(W^+) + \vec{P}(W^-) \qquad (37)$$
$$\vec{P}(\ell^+) + \vec{P}(\nu_\ell) + \vec{P}(q) + \vec{P}(\bar{q}) = 0$$

$$E_{\ell^+} + E_{\nu_\ell} + E_q + E_{\bar{q}} = \sqrt{s} = 2E_{beam}. \qquad (38)$$

Decay to $\ell\nu\ell\nu$ are of limited use because at least two neutrinos are undetected. The W decay products are paired up to give reconstructed W mass estimates. A substantial improvement is made in the mass resolution for both $q\bar{q}q\bar{q}$ and $q\bar{q}\ell\nu$ channels by applying a kinematic fit, constraining the total energy and momentum in the event to be that of the known colliding electron-positron system as shown in Eq.s 37 and 38, and making a small correction for possible unobserved initial-state radiation.

A typical reconstructed mass distribution from the kinematic fit are shown in Figure 13, for the $q\bar{q}\ell\nu$ channel. A clear W mass peak is observed with low background. The W mass is extracted from the measured W masses in each data event using a Monte Carlo technique, the details of which differ from one experiment to another. The Monte Carlo techniques have in common that they use full detector simulations to correct for the effects of finite detector acceptance and resolution, as well as initial-state radiation. An example of the results obtained from the fits are shown in Figure 13 (histogram). For all of these fits, the W width is taken to have its expected Standard Model dependence on the W mass. The combined W mass from direct reconstruction, taking into account all correlations including those between the $W^+W^- \to q\bar{q}\ell\bar{\nu}$ and $W^+W^- \to q\bar{q}q\bar{q}$ channels, gives

$$M_W = 80.428 \pm 0.030(\mathrm{stat.}) \pm 0.036(\mathrm{syst.})\ \mathrm{GeV}, \qquad (39)$$

with a χ^2/d.o.f of 27.1/29, corresponding to a χ^2 probability of 57%. Table 6 summarizes the combined result from each experiment at LEP-2. The results

Table 6: Summary of the W mass measurements from direct reconstruction ($\sqrt{s} = 172 - 202$ GeV) at LEP-2. Results are given for $W^+W^- \to q\bar{q}\ell\bar{\nu}$ and $W^+W^- \to q\bar{q}q\bar{q}$ channels. The χ^2 per d.o.f is 27.1/29.

Experiment	M_W (GeV)
ALEPH	80.449 ± 0.065
DELPHI	80.380 ± 0.071
L3	80.362 ± 0.078
OPAL	80.486 ± 0.066
Total	80.428 ± 0.047

are consistent with the W mass extracted from the measurement of the W pair threshold cross-section at 161 GeV (see Figure 4):

$$M_W = 80.40 \pm 0.20(\text{stat.}) \pm 0.03(\text{syst.}) \text{ GeV}. \tag{40}$$

The overall LEP average W mass measurement obtained is:

$$M_W = 80.427 \pm 0.046 \text{ GeV}. \tag{41}$$

The width of the W mass distributions shown in Figure 13 has components from the true W width and from detector resolution. In many events, the mass resultion is comparable to, or better than, the true width. It is consequently possible to measure directly both the W mass and width, and in practice the two results are little correlated. The combined result is

$$\Gamma_W = 2.12 \pm 0.20 \text{ GeV}. \tag{42}$$

W branching fraction, W mass and width from the Tevatron at Fermilab

At the Tevatron, the W bosons are only detected in their decays to $e\nu$ and $\mu\nu$ because the decay to qq' is swamped by the QCD dijet background whose cross section is over an order of magnitude higher than the mass range of interest. Also one does not know the event $\hat{s}$ and one can not determine the longitudinal (parallel to the beam direction) neutrino momentum because a significant fraction of the products from the $p\bar{p}$ interaction are emitted at small angle to the beam pipe where there is no instrumentation. Consequently, one must determine the W mass from transverse (perpendicular to the beam direction) quantities [7], *i.e.* : the transverse mass M_T, the charged lepton

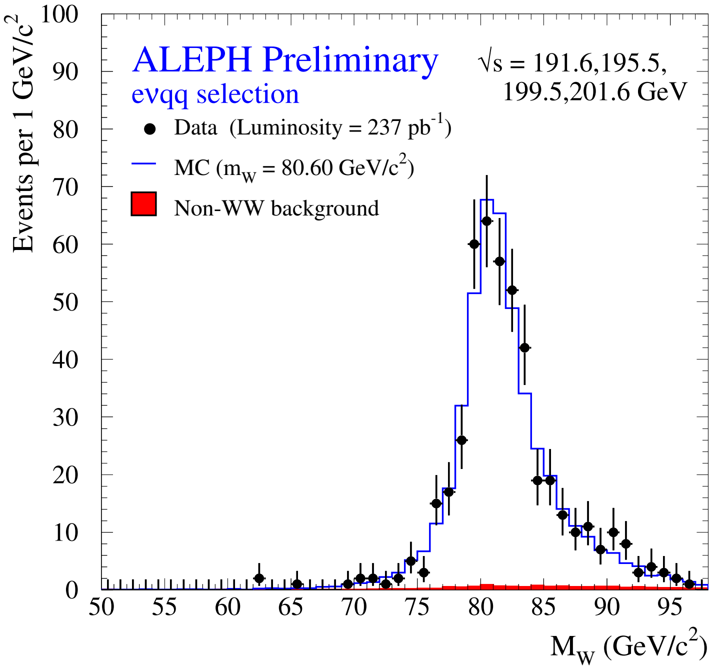

Figure 13: Reconstructed W mass distribution compared to the best fit for the $e^+e^- \to W^+W^- \to e^+\nu q\bar{q}'$ channel at the ALEPH experiment at LEP-2.

transverse momentum P_T^ℓ, or the neutrino transverse momentum P_T^ν (or the missing transverse energy $\not{E}_T$). $\not{E}_T$ is inferred from a measurement of P_T^ℓ and the remaining P_T in the detector, denoted by $\vec{u}$, *i.e.*

$$\vec{P}_T^W + \vec{P}_T^{gluons} = 0 \tag{43}$$
$$\vec{P}_T^\ell + \vec{P}_T^\nu + \vec{u} = 0 \quad \text{or} \quad \vec{P}_T^\nu = \vec{\not{E}}_T = -(\vec{P}_T^\ell + \vec{u}).$$

The following cartoon demonstrates kinematics of W boson production and decay, as viewed in the plane transverse to the antiproton-proton beams, where the recoil energy vector $\vec{u}$ is the sum of the transverse energy vectors $\vec{E}_T^i$ of the particles recoiling against the W:

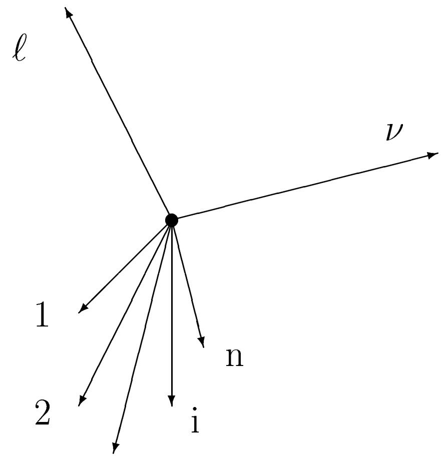

$$\vec{u} = \Sigma_{i=1}^{n} \vec{E}_T^i$$

$\vec{u}$ receives contributions from two sources: first, the so-called W recoil, *i.e.* the particles arising from initial state QCD radiation from the $q\bar{q}$ legs producing the hard scatter, and, second, contributions from the spectator quarks ($p\bar{p}$ remnants) and additinal soft scatters by $p'\bar{p}'$ which occur in the same crossing as the hard scatter. This second contribution is generally referred to as the underlying-event contribution. Experimentally, these two contributions cannot be distinguished. Owing to the contribution from the underlying-event, the missing transverse energy resolution has a significant dependence on the instantaneous $p\bar{p}$ luminosity.

Transverse mass of W, M_T^W, is defined as

$$M_T^W = \sqrt{2P_T^{\ell}P_T^{\nu}(1 - \cos\phi)} \tag{44}$$

where ϕ is the angle between $\vec{P_T^{\nu}}$ and $\vec{P_T^{\ell}}$. M_T is to first order independent of the transverse momentum of the W (P_T^W) where as P_T^{ℓ} is linearly dependent on P_T^W. For this reason, and at the Tevatron luminosities where the effect of the $\not\!\!E_T$ resolution is not too severe, the transverse mass is the preferred quantity to determine the W mass. However, the W masses determined from the P_T^ℓ and $\not\!\!E_T$ distributions provide important cross-checks on the integrity of the M_T result because the three measurements have different systematic uncertainties. Figure 14 and 15 show the transverse mass (M_T^W) and lepton transverse momentum (P_T^ℓ) distributions of W events.

The W mass at the Tevatron is determined through a precise simulation of the transverse mass line-shape, which exhibits a Jacobian edge at $M_T \sim M_W$. The simulation of the line-shape relies on a detailed understanding of the detector response and resolution to both the charged lepton and the recoil particles. This in turn requires a precise simulation of the W production and decay. The similarity in the production mechanism and mass of the W and Z bosons is exploited in the analysis to constrain many of the systematic uncertainties in the W mass analysis. The lepton momentum and energy scales are determined by a comparison of the measured Z mass from $Z \to e^+e^-$ and $Z \to \mu^+\mu^-$ decays with the value measured at LEP. The simulation of the W P_T and the detector response to it are determined by a measurement of the Z P_T which is determined precisely from the decay leptons and by a comparison of the leptonic (from the Z decay) and non-leptonic E_T quantities ($\vec{u}$) in Z events. The reliance on the Z data means that many of the systematic uncertainties in the W mass analyses are determined by the statistics of the Z sample.

The W and Z events in these analyses are selected by demanding a single isolated high P_T charged lepton in conjunction with missing transverse energy (W events) or a second high P_T lepton (Z events). Depending on the analyses, the $\not\!\!E_T$ cuts are either 25 or 30 GeV and the lepton P_T cuts are similarly 25 or 30 GeV. In total, $\sim 84k$ events are used in the W mass fits and $\sim 9k$ Z events are used for calibration.

The Tevatron average W mass measurement obtained is [8]

$$M_W = 80.448 \pm 0.062 \text{ GeV}. \tag{45}$$

The Tevatron experiments determine the width by a one parameter likelihood fit to the high end of the transverse mass distribution (see Figure 16). Detector resolution effects fall off in a Gaussian manner such that at high transverse masses ($M_T > 120$ GeV), the distribution is dominated by the Breit-Wigner behavior of the cross section. In the fit region, CDF has 750 events in the electron and muon channels combined. The result [9] is

$$\Gamma_W = 2.055 \pm 0.125 \text{ GeV}. \tag{46}$$

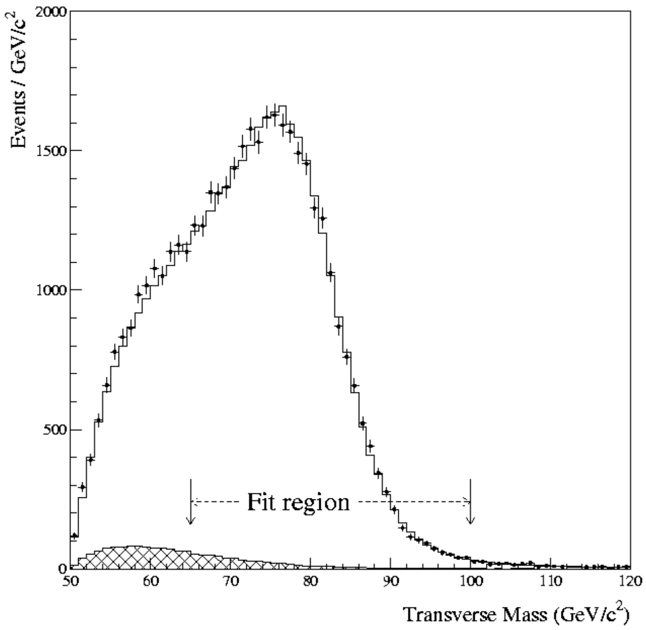

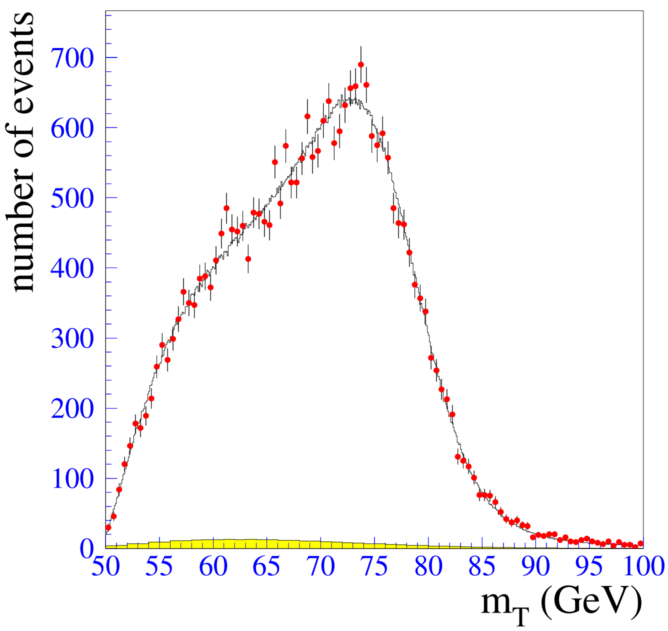

Figure 14: W Transverse mass distributions compared to the best fits for the $W \to e\nu$ channel from the CDF experiment (Top) and the DØ experiment (Bottom).

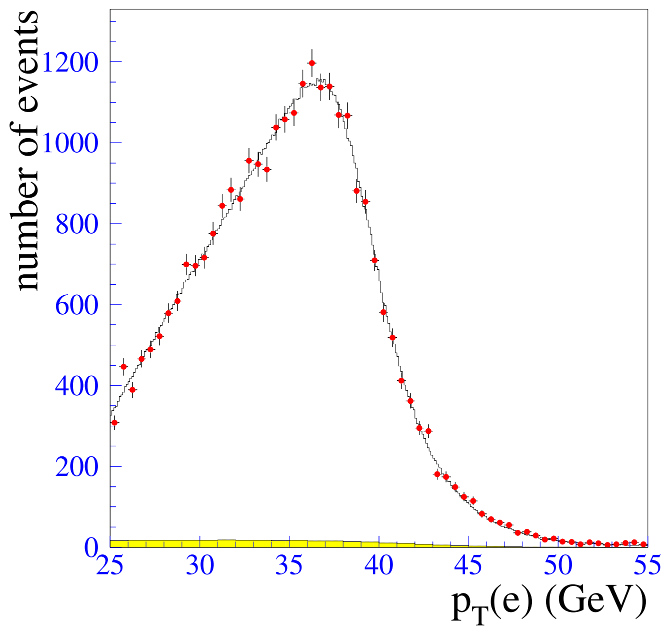

Figure 15: The electron transverse momentum distribution compared to the best fit for the $W \to e\nu$ channel from the DØ experiment.

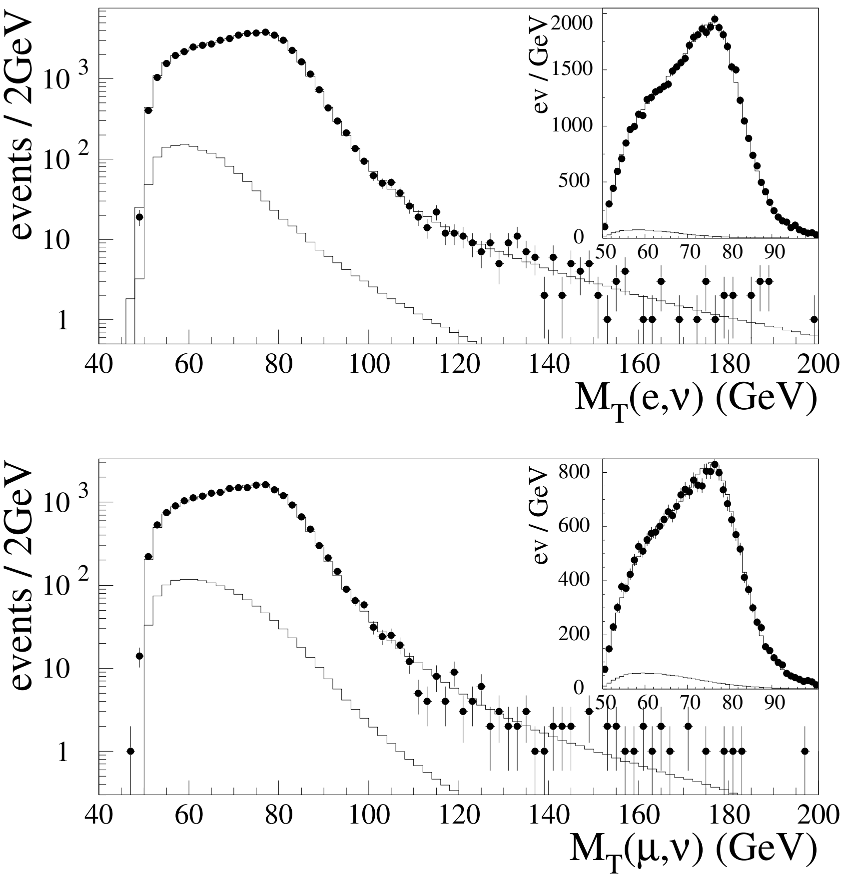

Figure 16: Transverse mass spectra (filled circles) for $W \to e\nu$ (Top) and $W \to \mu\nu$ (Bottom) data from the CDF experiment, with best fits superimposed as solid curves. The lower curve in each graph shows the sum of estimated backgrounds. Each inset shows the $50 - 100$ GeV region on a linear scale.

At LEP-2, the W branching fractions are determined by an explicit cross section measurement, while at the Tevatron they are determined from a measurement of a cross section ratio. Specifically, the W branching fraction can be written as:

$$\sigma \cdot Br(W \to e\nu) = \frac{\sigma_W}{\sigma_Z} \cdot \frac{\Gamma(Z \to ee)}{\Gamma_Z} \cdot \frac{1}{R} \tag{47}$$

where

$$R = \frac{\sigma_W \cdot Br(W \to e\nu)}{\sigma_Z \cdot Br(Z \to ee)} \tag{48}$$

is the measurement made at the Tevatron. This determination thus relies on the LEP-1 measurement of the Z branching fractions and the thoretical calculation of the ratio of the total Z and W cross sections. The Tevatron measurement $Br(W \to e\nu) = (10.43 \pm 0.25)\%$ is now becoming systematics limited. In particular, the uncertainty due to QED radiative corrections in the acceptance calculation and in σ_W/σ_Z contributes 0.19% to the total systematic uncertainty of 0.23%. The corresponding measurement from LEP-2 is $Br(W \to e\nu) = (10.62 \pm 0.20)\%$.

The large sample of W events at the Tevatron has also allowed a precise determincation of g_τ/g_e through a measurement of the ratio of $W \to \tau\nu$ to $W \to e\nu$ cross sections. The latest Tevatron measurement of this quantity is $g_\tau/g_e = 0.99 \pm 0.024$, in good agreement with the Standard Model prediction of unity and the LEP-2 measurement of $g_\tau/g_e = 0.101 \pm 0.022$.

W mass prediction from NuTeV at Fermilab

Neutrino scattering experiments have contributed to our understanding of electroweak physics for more than three decades. Early determinations of $\sin^2\theta_W$ served as the critical ingredient to the Standard Model's successful prediction of the W and Z boson masses. More precise investigations in the late 1980s set the first useful limits on the top quark mass. The recent NuTeV measurement of the electroweak mixing angle from neutrino-nucleon scattering represents the most precise determination to date. The result is a factor of two more precise than the previous most accurate νN measurement [10].

In deep inelastic neutrino-nucleon scattering, the weak mixing angle can be extracted from the ratio of neutral current (NC) to charged current (CC) total cross sections;

$$R^- = \frac{\sigma(\nu_\mu N \to \nu_\mu X) - \sigma(\bar{\nu}_\mu N \to \bar{\nu}_\mu X)}{\sigma(\nu_\mu N \to \mu^- X) - \sigma(\bar{\nu}_\mu N \to \mu^+ X)} \tag{49}$$

$$= \frac{R^{\nu} - rR^{\bar{\nu}}}{1-r} = \frac{1}{2} - \sin^2\theta_W.$$

where $R^{\nu} = \sigma(\nu_\mu N \to \nu_\mu X)/\sigma(\nu_\mu N \to \mu^- X)$. Because R^- is formed from the difference of neutrino and anti-neutrino cross sections, almost all sensitivity to the effects of sea quark scattering cancels. This reduces the error associated with heavy quark production (principally due to the imprecise knowledge of the charm quark mass) by roughly a factor of eight relative to the previous analysis. The substantially reduced uncertainties, however, come at a price. The ratio R^- is difficult to measure experimentally because neutral current neutrino and anti-neutrino events have identical observed final states.

From the νN interactions, 386 k NC and 919 k CC events are recorded and from the $\bar{\nu}$N interactions, 89 k NC and 210 k CC events. The extracted value of $\sin^2\theta_W$ (on-shell) $= 0.2254 \pm 0.0021$ which can be translated in to an M_W value of $80.25 \pm 0.1(\text{stat.}) \pm 0.05(\text{syst.})$ GeV, where the systematic error also receives a contribution from the unknown Higgs mass.

Summary of W mass, width, and branching fraction measurements

The LEP-2 mass values are compared with the Tevatron values in Figure 17. They are in excellent agreement despite being measured in very different ways with widely different sources of systematic error. The systematics at LEP-2 are dominated by the uncertainty in the beam energy (which is used as a constraint in the mass fits) and by the modeling of the hadronic final state, particular for the events where both W bosons decay hadronically. At the Tevatron, the systematics are dominated by the determination of the chareged lepton energy scale and Monte Carlo modeling of the W production, in particular its P_T and P_Z distribution. At the Tevatron, one can not use a beam energy constraint to reduce the sensitivity of the W mass to the absolute energy (E) and momentum (p) calibration of the detector. Any uncertainty in the detector E, p scales thus enters directly as an uncertainty in the Tevatron W mass. This means that the absolute energy and momentum calibration of detectors must be known to better than 0.01%. By contrast at LEP, an absolute calibration of 0.5% is sufficient. These thus provide welcome complementary determinations of the W mass. These direct measurements are also in good agreement with the indirect measruement from NuTeV and the prediction based on fits to existing, non W, electroweak data (the Z parameters).

There is also good agreement between the LEP-2 and Tevatron measurements on the W width and branching fraction.

Table 7 summarizes the W parameter measurements at LEP-2 and the Tevatron.

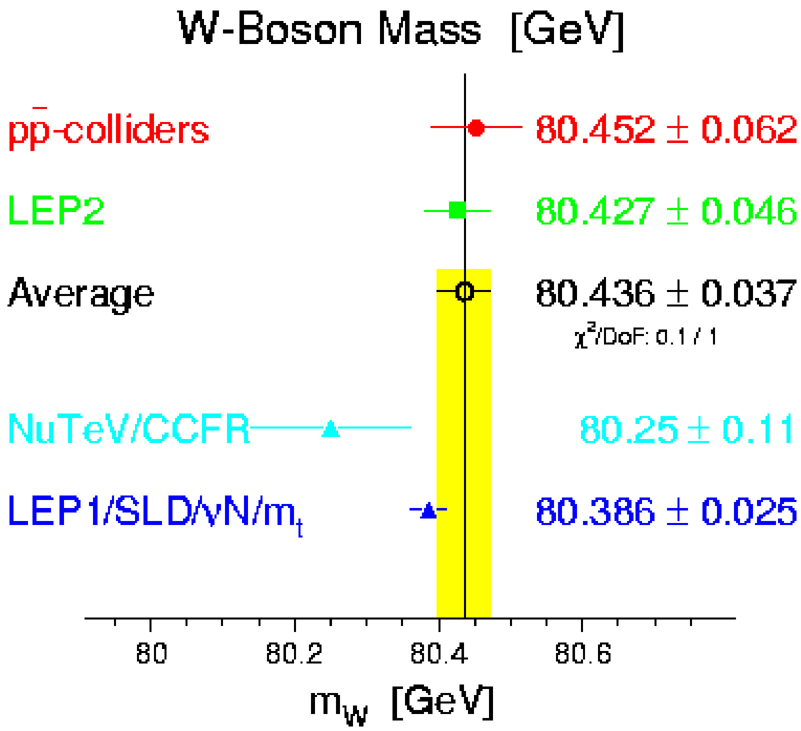

Figure 17: M_W measurements and the prediction from the electroweak measurements including $M_{\rm top}$.

Table 7: Summary of the W and top-quark parameter measurements at LEP-2 and the Tevatron.

Parameter	LEP-2	Tevatron
M_W	80.427 ± 0.046 GeV	80.448 ± 0.062 GeV
Γ_W	2.12 ± 0.20 GeV	2.055 ± 0.125 GeV
$Br(W \to \ell\nu)$	$(10.74 \pm 0.10)\%$ $(e+\mu+\tau)$	$(10.43 \pm 0.25)\%$ (e)
M_{top}	–	174.3 ± 5.1 GeV

Top-quark parameters

The top quark discovery [2] at the Tevatron in 1995 was the culmination of a search lasting almost twenty years. The top quark is the only quark with a mass in the region of the electroweak gauge bosons and thus a detailed analysis of its properties could possibly lead to information on the mechanism of electroweak symmetry breaking. In particular, its mass is strongly affected by radiative corrections involving the Higgs boson. The emphasis in top quark studies at the Tevatron has been to make the most precisie measurement of the top quark mass. Substantial progress has been made in bringing the mass uncertainty down from > 10 GeV, at the point of discovery, to 5.1 GeV in 1999.

In the Standard Model, a top quark decays $\sim$100% of the time to Wb. If both W's decay to qq', the final state from $t\bar{t}$ is $qq'qq'b\bar{b}$ and the event sample is referred to as "all-hadronic". Conversely, the "di-lepton" event sample is realized by selecting an $\ell^+\nu\ell^-\bar{\nu}b\bar{b}$ final state, where both W's have decayed leptonically (to e or μ). The "lepton+jet" event sample is one in which one W has decayed hadronically and the other leptonically. The precision with which the top quark mass can be measured with each sample depends on the branching fractions, the level of background and how well constrained the system is. The all hadronic sample has the largest cross section, but has a large background from QCD six jet events ($N_{signal}/N_{background} \sim 0.3$), while the di-lepton sample has a small background ($N_{signal}/N_{background} \sim 4$), but suffers from a small cross section and the events are "under-constrained" because they contain two neutrinos. The optimum channel in terms of event sample size, background level and kinematic information content is the lepton+jet channel. Indeed, this channel has a weight of $\sim$80% in the combined Tevatron average.

Figure 18 shows the reconstructed mass distribution using the lepton+jet event sample from the CDF experiment. The Tevatron combined value [5] is determined using lepton+jet, di-lepton, and all-hadronic data (see Figure 19) and accounting for all correlations between the measurements. The two experiments have assumed a 100% correlation on all systematic uncertainties related to the Monte Carlo models. The uncertainty in the Monte Carlo model of the QCD radiation is one of the largest systematic uncertainties. This error source will require a greater understanding if the top mass precision is to be significantly improved in the next Tevatron run (Run II). The other dominant systematic error is the determination of the jet energy scale which relies on using in-situ control samples such as Z+jet and γ+jet events. In Run II, due to significant improvements in the trigger system, both experiments should be able to accumulate a reasonable sample of $Z \to b\bar{b}$ events which will be of great assistance in reducing the uncertainty in the b-jet energy scale.

The top-quark mass measurments from the CDF and DØ experiments with various channels are summarized in Figure 19. The combined Tevatron mass value [5] is

$$\begin{aligned} M_{top} &= 174.3 \pm 3.2(\text{stat.}) \pm 4.0(\text{syst.})\ \text{GeV} \\ &= 174.3 \pm 5.1\ \text{GeV}. \end{aligned} \tag{50}$$

This measurement is a supreme vindication of the Standard Model, which, based on other electroweak measurements, predicts a top mass of :

$$M_{top} = 172^{+14}_{-11}\ \text{GeV}. \tag{51}$$

Of all the quark masses, the top quark is now the best measured.

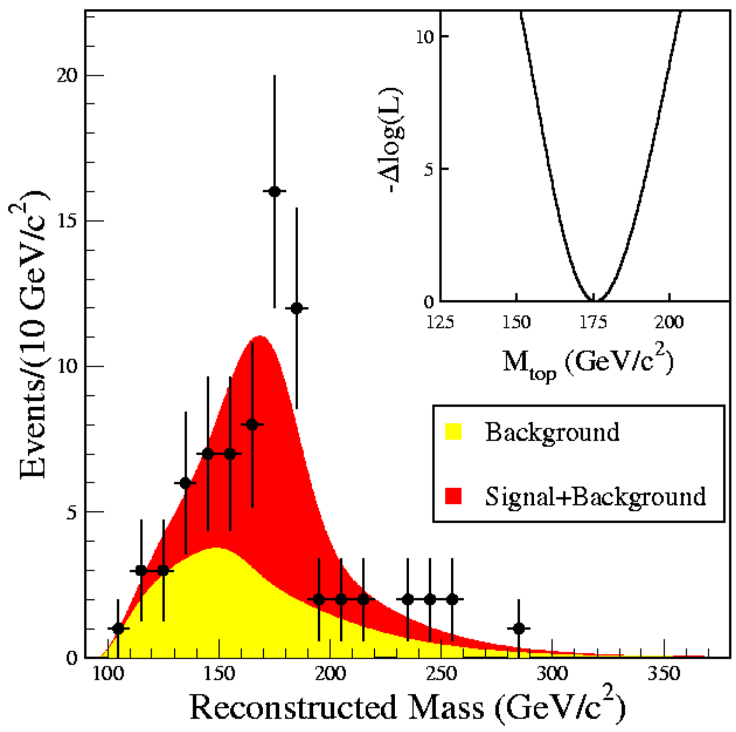

Figure 18: The reconstructed top quark mass distribution compared to the best fit for the $t\bar{t} \to (W^+b) + (W^-\bar{b}) \to (\ell^+\nu b) + (q\bar{q}'\bar{b})$. The plot also shows the level of background.

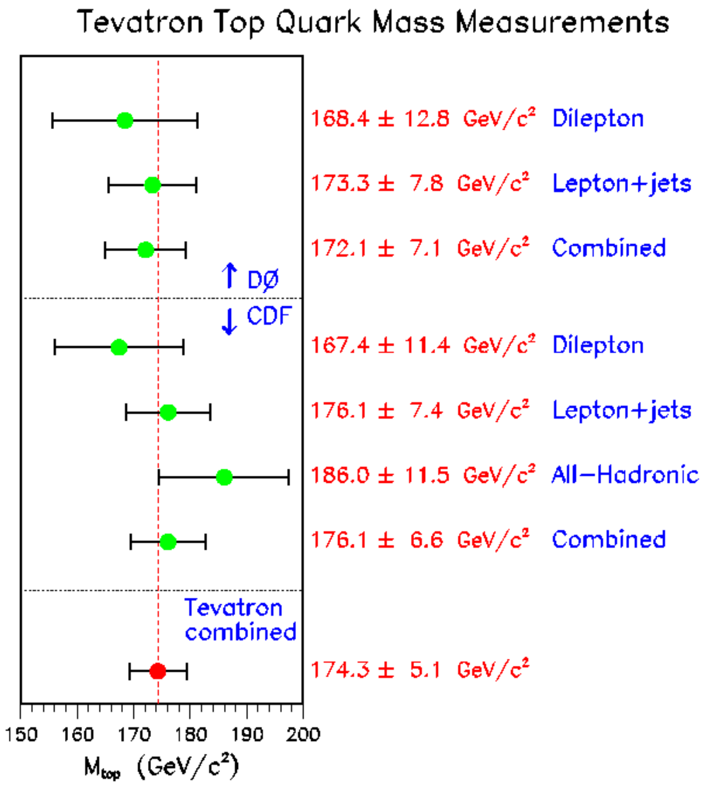

Figure 19: The summary of the top-quark mass measurements from the CDF and DØ experiments at the Tevatron.

Summary and Outlook

With the current uncertainties, the measurements of the W mass and top-quark mass start to provide an interesting further test of the Standard Model relative to precision electroweak measurements at the Z resonance. This is illustrated in Figure 20; the predicted W and top masses extracted from fits to lower electroweak data are consistent with the direct measurements from LEP-2 and Tevatron, and the precision of the measurements is similar to that of the prediction. From the overlaid curves showing the Standard Model expectation as a function of the Higgs boson mass, it is further evident that both the precise lower energy measurements, and the direct W and top mass measurements favor a Standard model Higgs boson in the relatively low mass region (see Figure 21). The 95% confidence level upper limit on M_H (taking the band into account) is 165 GeV. The lower limit on M_H of approximately 113 GeV obtained from direct searches[13] has not been used in this limit determination.

For LEP-1, LEP-2 and NuTeV, no further data are planned. In contrast, the Tevatron has undergone a major luminosity upgrade augmented with substantial improvements in the collider's detectors. At least 2 fb^{-1} is expected per experiment at an increased center of mass energy of 2 TeV in three years. It is expected that both the top quark mass and W mass measurements will become limited by systematic uncertainties. The statistical part of the Tevatron W mass error in the next run will be $\sim$10 MeV, where this also includes the part of the systematic error which is statistical in nature such as the determination of the charged lepton E and p scales from Z events. At present the errors non-statistical in nature contribute 25 MeV out of the total Tevatron W mass error of 60 MeV. A combined W mass error is expected to be $20-30$ MeV. The W width is expected to be determined with an uncertainty of $20-40$ MeV. The statistical uncertainty on the top quark mass will be $\sim$1 GeV. The systematic error arising from the uncertainties in the jet energy scale and modeling of QCD radiation are expected to be the dominant errors, with a total error value of $2-3$ GeV per experiment expected.

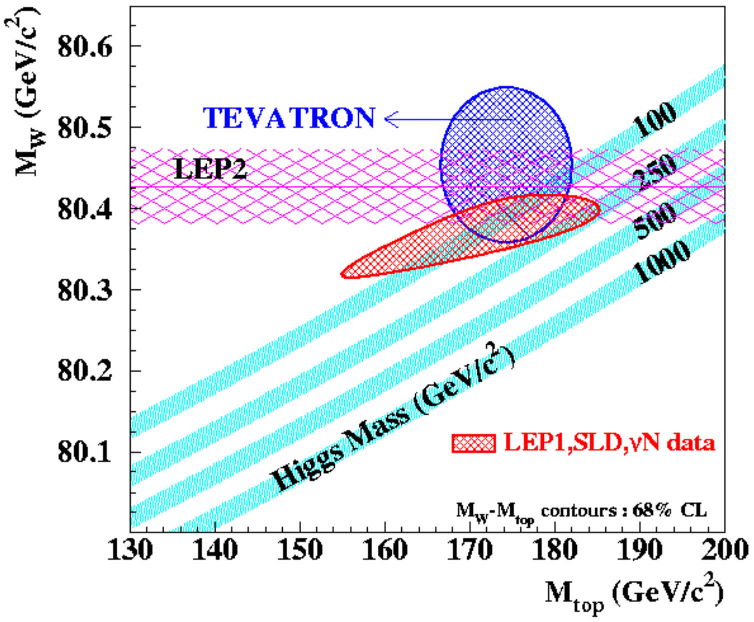

Figure 20: The direct measurements of the W and top quark mass from the Tevatron experiments, and the direct measurement of the W mass from the LEP-2 experiments and the indirect W and top mass measurement from LEP, SLC, and Tevatron neutrino experiments. The curves are from a calculation of the dependence of M_W on M_{top} in the Standard Model using several Higgs boson masses. The band on each curve is the uncertainty obtained by folding in quadrature uncertainties on $\alpha(M_Z^2)$, $\alpha_s(M_Z^2)$, and M_Z (Reference 11). The dominant contribution to the band width comes from the uncertainty on $\alpha(M_Z^2)$, $\Delta\alpha_{had}^{(5)}(M_Z^2)$, the contribution of light quarks to the photon vacuum polarisation.

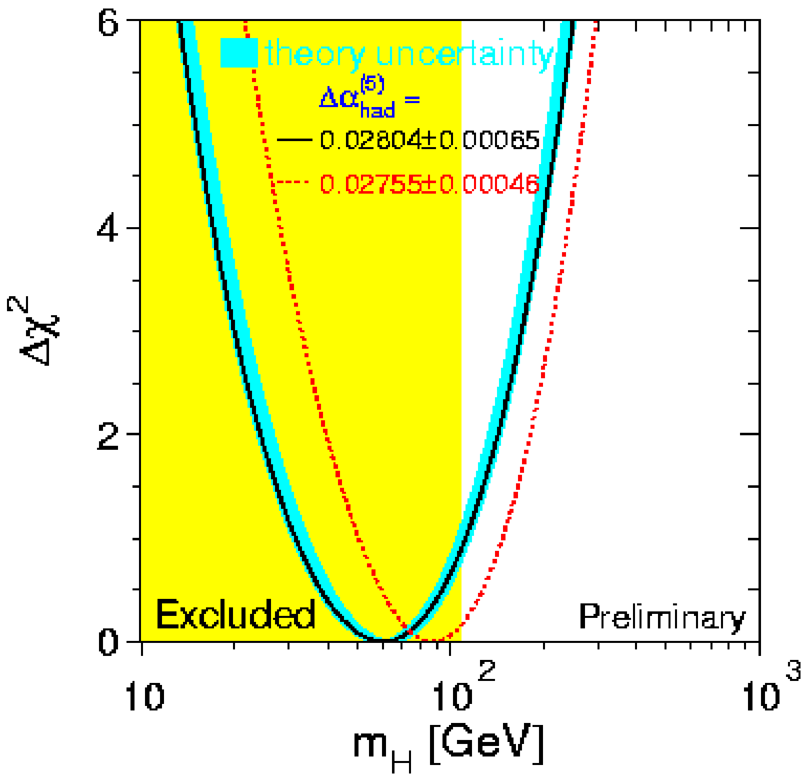

Figure 21: $\Delta\chi^2 = \chi^2 - \chi^2_{min}$ *vs.* M_H curve. The line is the results of the fit using all the Electroweak measurements; the band represents an estimate of the theoretical error due to missing higher order corrections. The vertical band shows the 95% CL exclusion limit on M_H from the direct search. The dashed curve is the results obtained using the evaluation of $\Delta\alpha^{(5)}_{had}(M_Z^2)$ from Reference 12.

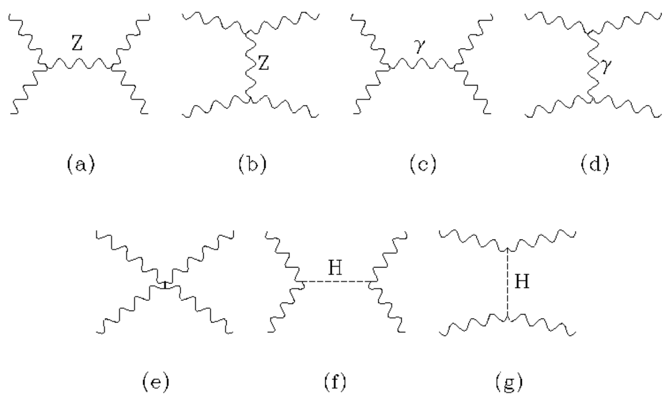

Figure 22: Tree-level diagrams for $W^+ + W^- \to W^+ + W^-$ scattering. Figure courtesy of "QCD and Collider Physics" by R.K. Ellis, W.J. Stirling and B.R. Webber.

4 Search of Electroweak Symmetry Breaking

As stated in Section 3, the Higgs sector can be probed by the precision electroweak measurements by means of radiative corrections. However, the nature of the symmetry breaking sector can only be established by its direct discovery and detailed study. The LEP-2 experiments have searched for a light Higgs boson upto ~115 GeV. In March 2001, the CDF and DØ experiments at the Tevatron will begin a high-luminosity run with considerable sensitivity to new physics, and offer promise for light-Higgs searches in the future. For more massive Higgs bosons, the focus of attention shifts to higher-energy colliders, in particular the LHC, where pp collisions will be studied at $\sqrt{s} = 14$ TeV, beginning in about 2006. Future possible e^+e^- linear colliders would offer complementary possibilities for the study of electroweak symmetry breaking.

4.1 Theoretical Constraints on the Higgs mass

The Higgs mass can not be too large; as it increases, the amplitude for WW scattering via Higgs exchange (see Figure 22 for the diagrams) becomes large and the contribution from the lowest-order diagrams exceeds the *perturbative* unitarity limit unless $M_H < 1$ TeV. It is also true that very massive Higgs bosons are wide resonant states (see Figure 23), and therefore their detection

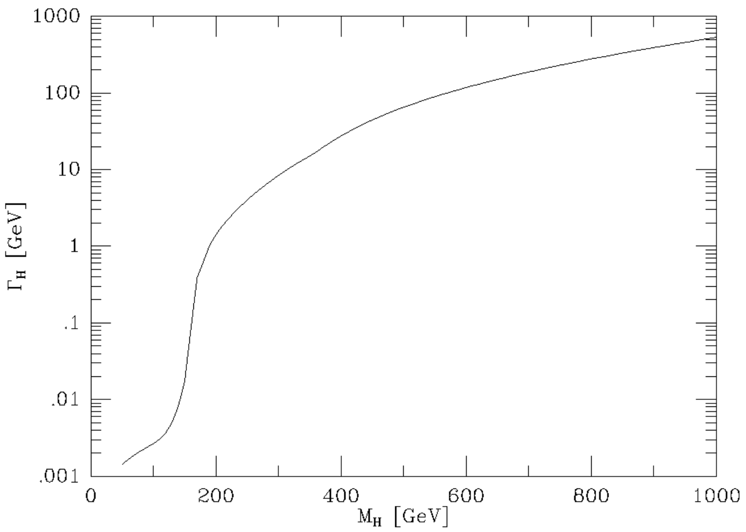

Figure 23: The total Higgs decay with for $M_{top} = 175$ GeV. Figure courtesy of "QCD and Collider Physics" by R.K. Ellis, W.J. Stirling and B.R. Webber.

in invariant mass distributions becomes difficult.

Another limit on M_H comes from consideration of the renormalized λ parameter which appears in the Higgs potential

$$V(\phi^+\phi) = \lambda(\phi^+\phi)^2 - \mu^2\phi^+\phi \tag{52}$$

where ϕ is the single complex doublet of scalar Higgs fields. With the parameters $\lambda, \mu^2 > 0$, this potential has a minimum at $\phi \neq 0$ and the vacuum expectation value v (= 246 GeV) is equal to $\sqrt{\mu^2/2\lambda}$. λ at low energy ($\lambda(v)$) can not be too large because it will increase with the scale and eventually a singularity will be reached. This gives an upper bound (Triviality bound) on the Higgs mass, which depends on the scale where new physics comes in. For example, $M_H < 175$ GeV if the new physics is at Λ_{planck} (10^{19} GeV), and $M_H < 1$ TeV if it is at $O(1$ TeV).

The Higgs vacuum will be unstable if the coupling strength between the top quark and the Higgs, Yukawa coupling g_t, is large so that g_t^2 is comparable to λ. This can be avoided if $M_H > 2(M_{top} - 110)$ GeV or $M_H > 130$ GeV (Vacuum Stability bound), assuming no new physics below the Planck scale.

In summary, the theoretical limits on the Higgs mass are $130 < M_H < 175$ GeV if new physics does not set in until the Planck scale, and $M_H < 1$ TeV if new physics comes in at $O(1\ \text{TeV})$. In other words, the Higgs mass can be almost arbitrary. See a detailed discussion on the Higgs mass constraints in Chris Quigg's lectures in this proceedings.

4.2 Searches for the Standard Model Higgs

Searches at LEP-2

The LEP-2 experiments have searched for the Higgs boson via the process $e^+e^- \to Z^* \to ZH \to (f\bar{f} + b\bar{b})$ or $(f\bar{f} + \tau\bar{\tau})$:

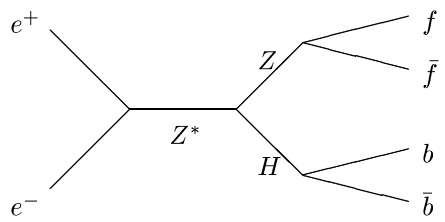

The final-state Z boson can be produced either on mass-shell if $\sqrt{s} > M_H + M_Z$, or off mass-shell if $\sqrt{s} < M_H + M_Z$. Figure 24 shows the cross section as a function of $\sqrt{s}$ for three different values of M_H. The LEP-2 collider went upto the center-of-energy of 208 GeV, higher than the design value. With this machine, the Higgs mass can be discoverd upto $\sim$110 GeV where Higgs decays mainly into $b\bar{b}$ or $\tau\bar{\tau}$ (see the branching fractions in Figure 25). At their highest energy, the 4 LEP-2 experiments have seen a 2.9 σ hint with $M_H = 115$ GeV (the excess is dominated by the ALEPH experiment) [14]. For instance, with a set of cuts which give the signal to background ratio of 2, the number of background events and the number of signal events with 115 GeV Higgs are estimated to be 1.72 and 3.03 (4 experiments combined), respectively. The number of candidates they observed is 4. With the same data, one can set the bound on the Higgs Mass; $M_H < 113$ GeV is excluded at 95% Confidence Level. The LEP-2 was shutdown in October 2000, passing the baton to the Tevatron for the Higgs searches (see the cartoon, Figure 26, made by the ALEPH experiment).

Searches at the Tevatron

At the Tevatron, the CDF and DØ experiments will begin a high-luminosity run in March 2001 with 10% increase in the center-of-mass energy, corresponding to $\sim$30% increase in the production cross section. Both experiments have

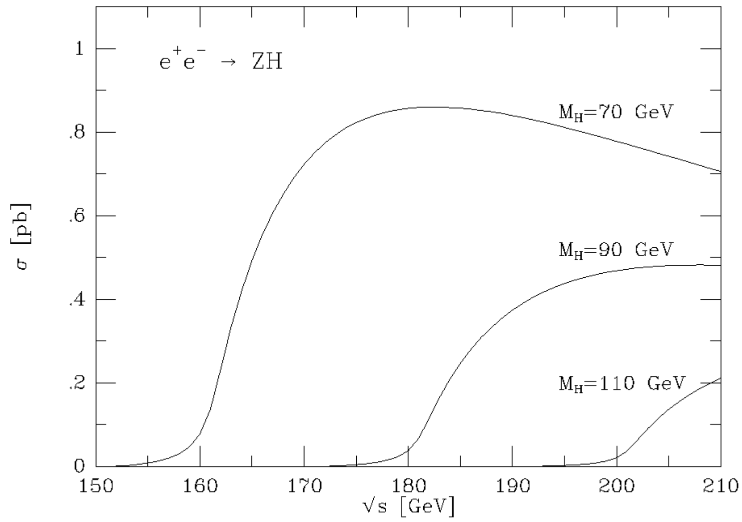

Figure 24: Cross section for ZH production at LEP-2. Figure courtesy of "QCD and Collider Physics" by R.K. Ellis, W.J. Stirling and B.R. Webber.

undergone major upgrades on their detectors, triggers, and data handling systems. These upgraded accelerator and experiments offer discovery potential of the light Higgs boson before the LHC turns on. Figure 27 shows the cross-sections as a function of the Higgs mass for various production mechanisms. For the Higgs lighter than $\sim$ 120 GeV, the search strategy is via the process $q\bar{q} \to V^* \to VH \to f\bar{f}b\bar{b}$,

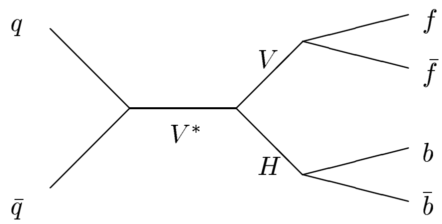

where V is W or Z. Although many more Higgs bosons are produced via $q\bar{q} \to H \to b\bar{b}$, they will be very difficult to detect due to large QCD background via $q\bar{q} \to g \to b\bar{b}$.

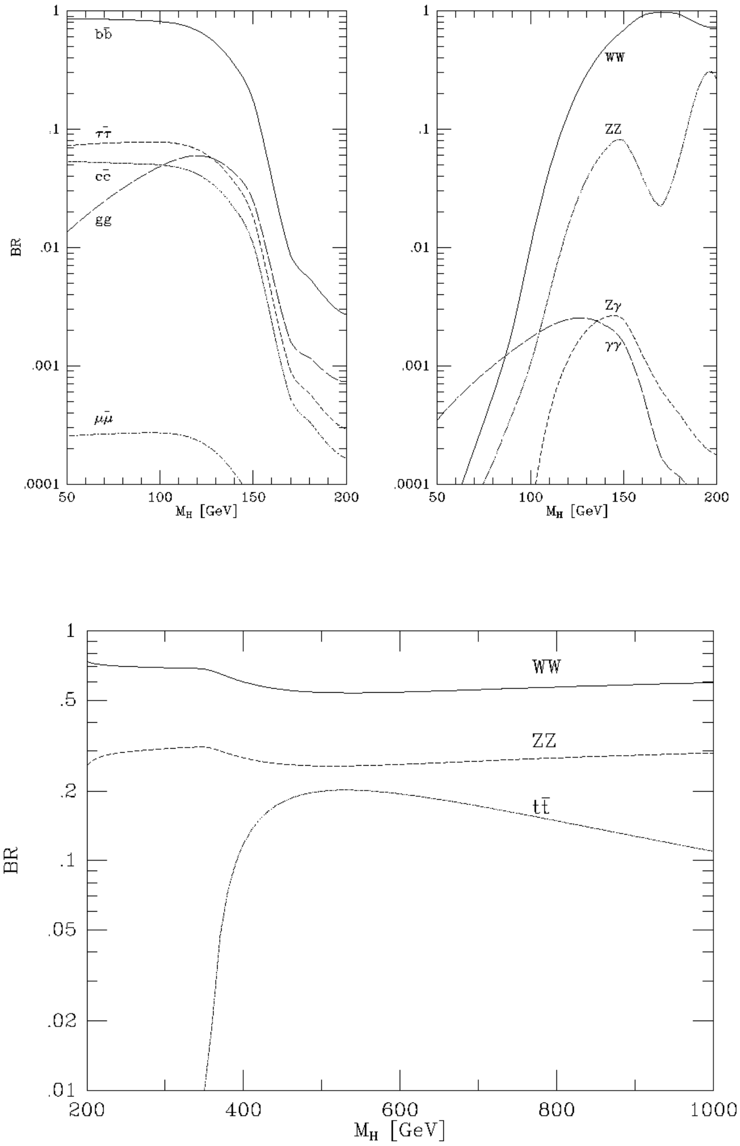

Figure 25: Branching fractions of the Standard Model Higgs boson for light Higgs (top) and heavy Higgs (Bottom). The top quark mass is 175 GeV. Figure courtesy of "QCD and Collider Physics" by R.K. Ellis, W.J. Stirling and B.R. Webber.

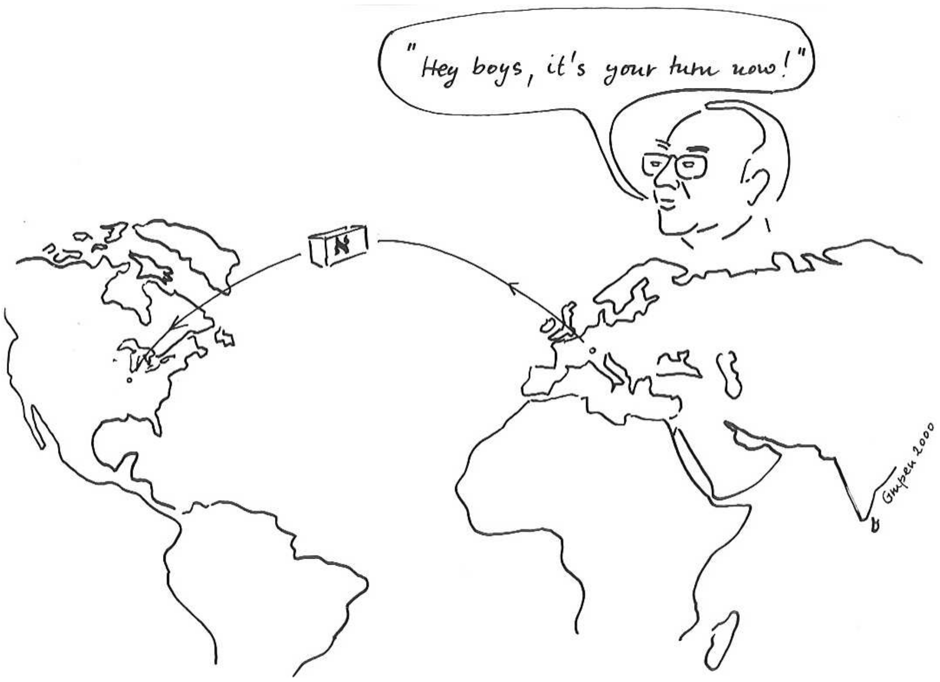

Figure 26: A cartoon made by the ALEPH experiment after the LEP-2 shutdown.

For the Higgs heavier than $\sim$ 130 GeV, $q\bar{q} \to H \to W^+W^{-*}$ or ZZ^* will be the dominant processes for the searches.

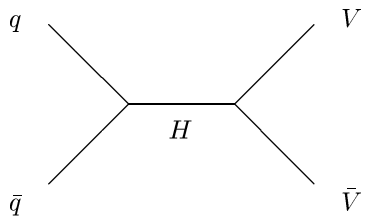

Lines in Figure 28 show the total luminosity required per experiment for 2σ, 3σ, and 5σ excesses due to the Higgs as a function of the Higgs mass. The Tevatron is expected to deliver $\sim$2 fb^{-1} per experiment in the first 3 years (called "Run IIa"). With the Run IIa data, the Tevatron experiments will observe a 2σ excess if the Higgs mass is 115 GeV. With further machine upgrade, CDF and DØ expect to have $\sim$10 − 15 fb^{-1} per experiment by year 2006 (called "Run IIb"). With this luminosity, they will see upto a 3σ excess over most of the region with $M_H < 180$ GeV.

Searches at LHC

For more massive Higgs bosons, we must wait for the LHC. The LHC will produce light Higgs bosons copiously (see Figure 29) but they will suffer from severe backgrounds (more severe than the Tevatron). One strategy is to look for $gg \to H \to \gamma\gamma$ events. The braching fraction of $H \to \gamma\gamma$ (see Figure 25) is extremely small (less than 1%), but backgrounds will be much smaller. For heavier Higgs bosons, the production cross section is smaller, but backgrounds are more manageable. The best process for this case could be via $gg \to H \to ZZ^* \to \ell^+\ell^-\ell^+\ell^-$. The invariant mass distributions for these two cases are shown in Figures 30 and 31.

4.3 Higgs Beyond the Standard Model

The Higgs mechanism, while it has many attractive features, is not without difficulties. There is, for example, a severe fine-tuning ('naturalness') problem associated with preventing the Higgs mass being renormalized up to some very high 'new-physics' or grand unification scale. Supersymmetry (SUSY) is one way of circumventing this difficulty while retaining the essential features of the Standard Model Higgs sector.

In the minimal supersymmetric model (MSSM), it is necessary to introduce two complex doublets of Higgs fields, and the masses and couplings of the

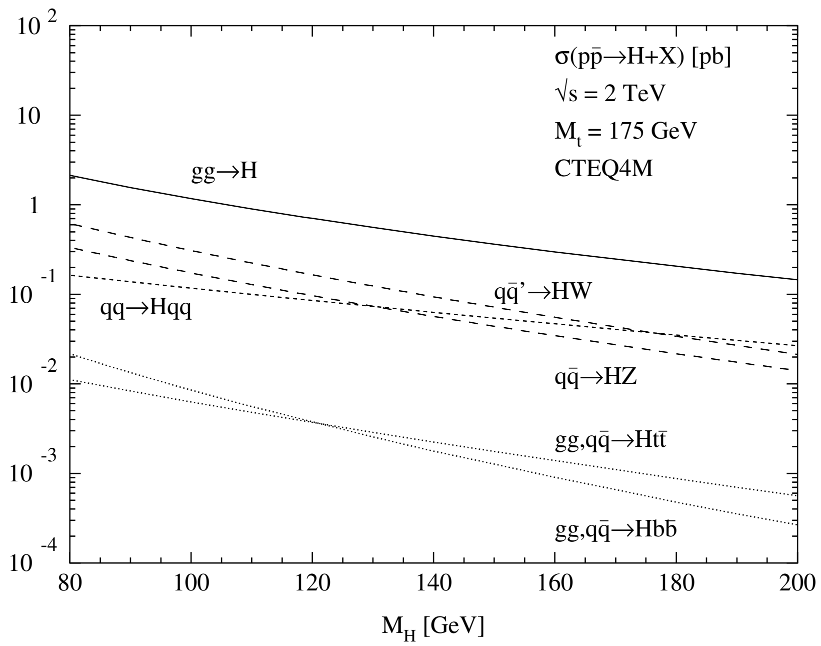

Figure 27: Higgs production cross sections at the Tevatron.

resulting five physical Higgs bosons are expressible (at leading order) in terms of just two parameters. The key feature of the minimal SUSY model is the existence of at least one neutral, scalar Higgs boson with a mass less then $O(150 \text{ GeV})$, the exact upper limit depending weakly on the parameters of the model on M_{top}. Note that a large fraction of SUSY models predict $M_{Higgs} <$ 130 GeV. In most respects, the lightest minimal SUSY Higgs boson behaves exactly like the Standard Model Higgs, and so the calculations and search strategies described in this section again apply.

Via loop diagrams, new particles make contributions to the electroweak parameters. Figure 32 shows the predicted $M_W - M_{top}$ region in the MSSM which is consistent with the current electroweak measurements.

5 Future Prospects

We will have possible senarios in this decade.

- We will discover the Higgs boson with $M_{Higgs} < 130$ GeV. This will lead

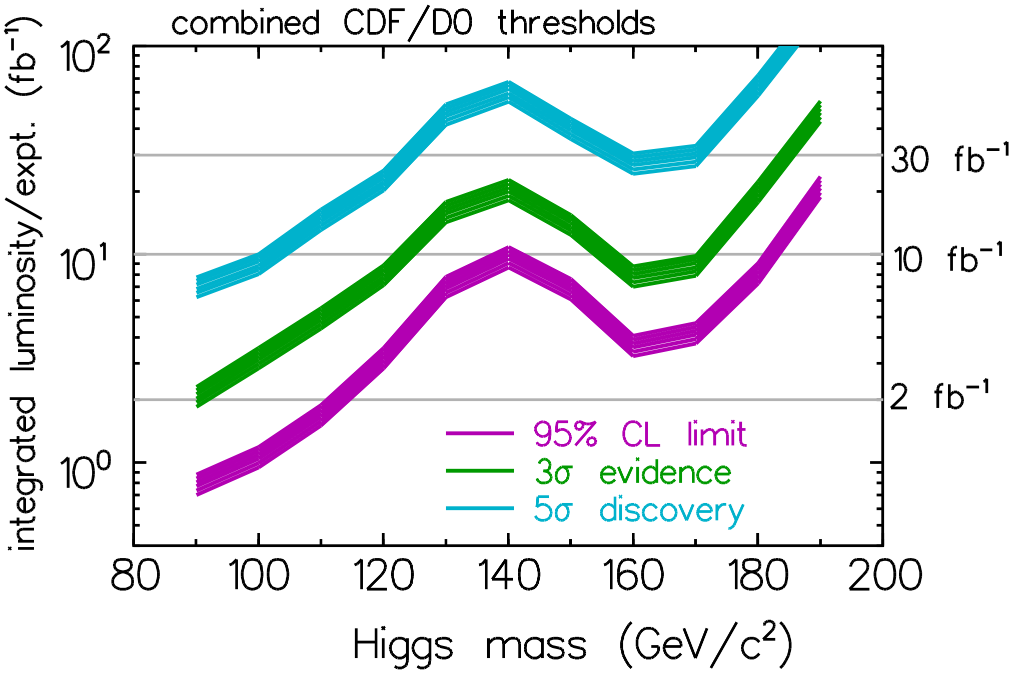

Figure 28: Higgs discovery potential at the Tevatron Run II.

to another question; is it the Standard Model Higgs ? If not, this will imply new physics.

- We will discover the Higgs boson with $M_{Higgs} > 130$ GeV. This will rule out a large fraction of SUSY models. This will lead to a question, "Will this agree with the indirect predicion from the electroweak precision measurements ?"

- We will not discover upto LHC. In this senario, we expect that detectable effects appear in the production rate and properties of W boson pairs at $\sim$1 TeV.

Whatever the outcome, it will be extremely interesting. At present, it is essentially an experimental question.

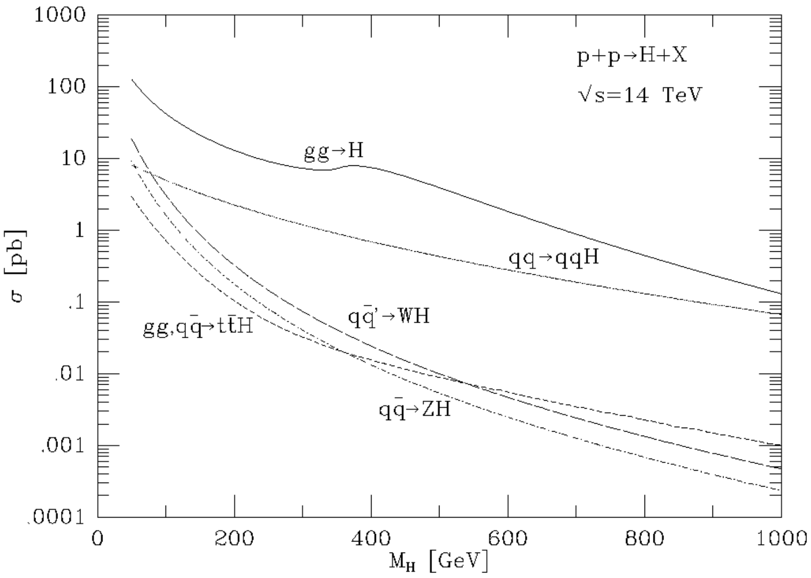

Figure 29: Higgs production cross section in *pp* collisions at the LHC. Figure courtesy of "QCD and Collider Physics" by R.K. Ellis, W.J. Stirling and B.R. Webber.

Acknowledgments

I would like to thank Jon Rosner who organized the TASI-2000 and edited Lecture Notes. I would also like to thank and acknowledge the collaborators of the CDF, D∅ and NuTev experiments, and the ALEPH, DELPHI, L3, OPAL, and SLD experiments. This work is supported by the U.S. Department of Energy.

References

1. G. Arnison *et al.* (UA1 Collaboration), PLB **122**, 103 (1983); M. Banner *et al.* (UA2 Collaboration), PLB **122**, 476 (1983)
2. F. Abe *et al.* (CDF Collaboration), PRL **74**, 2626 (1995), PRD **50**, 2966 (1994); S. Abachi et al. (D∅ Collaboration), PRL **74**, 2632 (1995).
3. A. Czarnecki and W.J. Marciano, Report BNL-HET-98/43, hep-ph/9810512.
4. The LEP Collaborations, the LEP Electroweak Working Group, the SLD

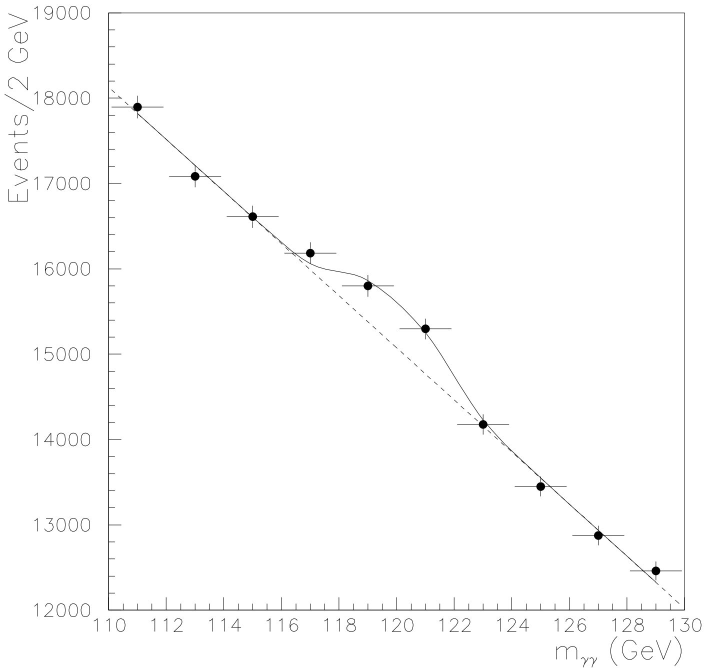

Figure 30: Expected $M_{\gamma\gamma}$ spectrum as simulated in the ATLAS detector at the LHC for M_H = 120 GeV and one year of data. The dotted line is background spectrum, and the solid line is background and signal combined spectrum. Figure courtesy of "QCD and Collider Physics" by R.K. Ellis, W.J. Stirling and B.R. Webber.

Heavy Flavour and Electroweak Working Group, hep-ex/0103048.

5. F. Abe *et al.* (CDF Collaboration), PRD **63**, 032003 (2001); F. Abe *et al.* (CDF Collaboration), PRL **82**, 271 (1999); B. Abbott *et al.* (D∅ Collaboration), PRD **58**, 052001 (1998).
6. C. Caso *et al.*, Eur. Phys. J. C3, 1 (1998).
7. V. Barger *et al.*, *Z. Phys.* C **21**, 99 (1983); B. J. Smith *et al.*, *Phys. Rev. Lett.* **50**, 1738 (1983).
8. J. Alitti *et al.* (UA2 Collaboration), *Phys. Lett.* B **276**, 246 (1992); T. Affolder *et al.* (CDF Collaboration), hep-ex/0007044 (submitted to Phys. Rev. **D**); S. Abachi *et al.* (D∅ Collaboration), PRL **84**, 222

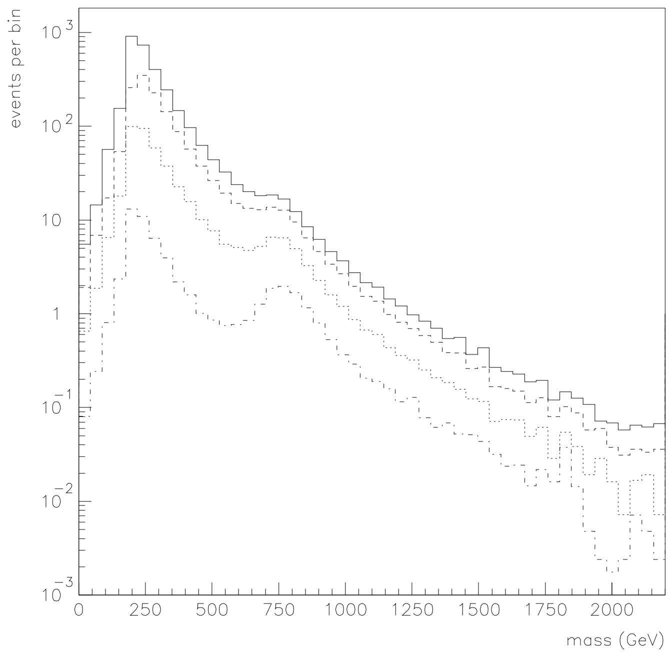

Figure 31: Expected M_{ZZ} spectrum as simulated in the ATLAS detector at the LHC for $M_H = 800$ GeV and one year of data. The different histograms repesent different selection cuts. Figure courtesy of "QCD and Collider Physics" by R.K. Ellis, W.J. Stirling and B.R. Webber.

(2000);

9. T. Affolder *et al.* (CDF Collaboration), submitted to PRL (2000).
10. K. S. McFarland, *et al.*, Eur. Phys. Jour. C31, 509 (1998).
11. M. Swartz, hep-ph/9509248; S. Eidelman, F. Jegerlehner, hep-ph/9502298
12. B. Pietrzyk, *The global fit to electroweak data,* talk presented at ICHEP2000, Osaka, July 27 - August 2, 2000. Preprint LAP-EXP-00.06.
13. K. Hoffman, *Year 2000 update for OPAL and LEP HIGGSWG results*, talk presented at ICHEP2000, Osaka, July 27 - August 2, 2000.
14. ALEPH Collaboration, CERN-EP/2000-138.

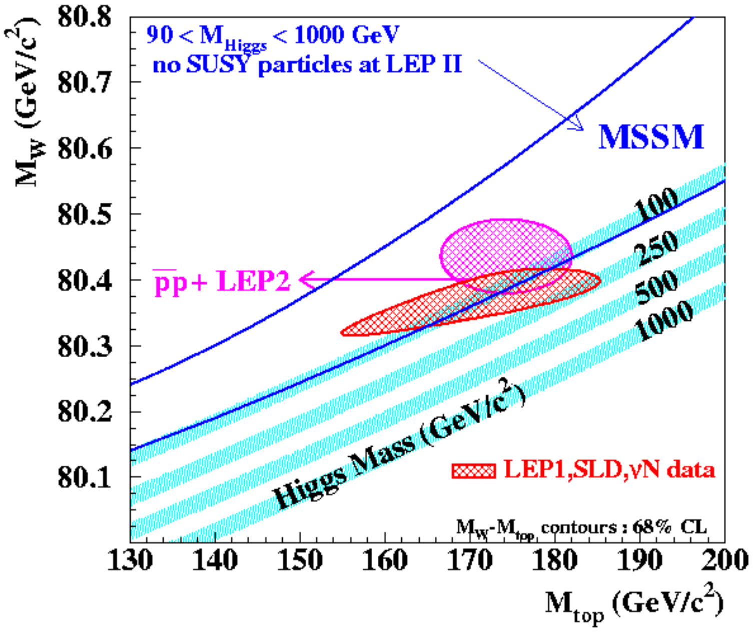

Figure 32: The direct and indirect measurements of the W and top quark mass from LEP, the Tevatron, and SLC overlaid with the allowed region from the MSSM model.